Post-Print

This is the accepted version of:

Multiphysics cross-section analysis of smart beams

Wenguo Zhu[a] and Marco Morandini[b]

[a]School of Aeronautic Science and Engineering, Beihang University, Beijing 100191, People's Republic of China; [b]Dipartimento di Scienze e Tecnologie Aerospaziali, Politecnico di Milano, Milano 20156, Italy

Abstract
The cross-section response of smart beams under electric, magnetic and thermal fields is investigated. The method predicts the generalized cross-section stiffness of prismatic smart beam, and allows recovering the three dimensional multiphysics fields variables. The semi-analytical procedure divides the contributions of the non-homogeneous governing equation into a homogeneous solution, which resorts to computing the de Saint-Venant solution, and a set of particular solutions which describe the beam cross-section behaviors when external electric potential, magnetic potential and boundary temperature are imposed. The generalized cross-section stiffness is computed by means of an energy equivalence equation.

KEYWORDS
multiphysics; beam; cross-section; magneto-electro-elastic; thermal, semi-analytical

1. Introduction

Smart materials do include piezoelectic, piezomagnetic and magneto-electro-elastic materials. They have controllable properties and can respond to external excitation, thus providing a new entry for engineers to improve the performance of structural systems. They are often exposed to multiphysics fields, such as electric field, magnetic field, mechanical field and sometimes temperature field, and they have the ability to transform one form of energy to another which makes them suitable for applications in vibration alleviation, sensing and actuating device, energy harvesting etc (Loewy, 1997; Chopra, 2002).

Many smart material applications make use of beams, slender structural elements for which one dimension is much larger than the other two dimensions. Smart beams have been used in smart helicopter rotor blades, adaptive wind turbine blades, morphing wings, and architectures (Loewy, 1997). Many pioneer works have been done to predict the behavior of smart beams. Besides computation that resorts to full three dimensional finite element analysis, these computation techniques can be classified into three main groups (Roy et al., 2007; Bauchau and Han, 2014): engineering methods that are based on certain a-priori kinematic assumptions, variational asymptotic methods (VAM) that are based on asymptotic expansions of the three dimensional quantities and finally

CONTACT: marco.morandini@polimi.it

semi-analytical methods that are resorting to computing the de Saint-Venant problem solutions.

Based on various a-priori kinematic assumptions, beam theories with different level of accuracy have been derived, such as widely used Euler-Bernoulli beam theory, classic beam theory associated with the de Saint-Venant theory of torsion and a set of refined beam theories accounting for transverse shear deformations and constrained wrappings (Hodges, 2006; Bauchau and Craig, 2009; Rafiee et al., 2017). Smart beams are modeled based on the above beam theories incorporating with the electro-mechanical coupling relationship. Piezoelectric beams exploiting Euler-Bernoulli beam theory were modeled by (Crawley and Anderson, 1990). A uniform strain theory was proposed to predict the static response of rectangular section beams by (Chen and Chopra, 1996) assuming that only bending (chord-wise bending is neglected) and torsional deformation do happen. Based on the Timoshenko beam theory with first order displacements field and a higher-order beam theory (Reddy, 1984), the smart beam governing differential equations in the form of state space equation were derived by (Aldraihem and Khdeir, 2000), and the Jordan canonical form was computed to obtain the analytical solution. A smart beam model using a layerwise (zigzig) theory was proposed by (Kapuria and Alam, 2006). Based on simple higher order shear deformation theory which allows parabolic shear strains, a finite element procedure for composite beam patched with piezoelectric device was developed in (Elshafei and Alraiess, 2013). Countless papers have been published on this subject, readers can refer to (Loewy, 1997; Chopra, 2002; Yang, 2007; Kapuria et al., 2010; Rafiee et al., 2017) for a detailed review.

The variational asymptotic method is based on (Berdichevskii, 1979) and was later developed by (Hodges, 2006) and his co-workers (Cesnik and Hodges, 1997; Yu, 2002). Taking advantage of the high aspect ratio of beams, VAM eliminates the less significant terms in the elastic formulation of three dimensional beam and splits the three dimensional nonlinear problem into a two dimensional linear cross-section analysis and a one dimensional nonlinear beam analysis without any a-priori kinematic assumptions. VAM was extended to model smart beams that are embedded with active fiber composites by (Cesnik and Palacios, 2003), but the electric field is assumed to be known and remains constant inside the active material domain. Later the procedure was refined by introducing a set of finite section deformation modes and electric modes that allow arbitrary definition of displacements and electric fields (Palacios and S. Cesnik, 2005). Following the general framework of VAM, an asymptotically correct classical beam model for smart structures was developed by (Roy et al., 2007), and later the beam model was refined to account for transverse shear effects (Roy and Yu, 2009). The fully coupled magneto-electro-elastic behavior of smart beam was investigated by (Wang and Yu, 2012) applying VAM; two kinds of electromagnetic fields were discussed, the first one varying along the beam axis, and the second one varying throughout the cross-section. The same authors also extended their work to take thermal effects into account (Wang and Yu, 2011).

Another category of method solves the de Saint-Venant problem, i.e. the elasticity solution of a three dimensional beam loaded only at its extremities. Giavotto (Giavotto et al., 1983) first developed a generalized numerical procedure for anisotropic beams with arbitrary geometry cross-section. The procedure leads to a second-order ordinary differential equation along the beam, whose solution is composed by two part, and in accordance to de Saint-Venant's principle, a polynomial part that is called "central solution", and a self-balanced exponential part which is called "extremity solution". Based on a semi-analytical method, in which the finite element mesh only discretizes the beam 2D cross-section, while the nodal displacements still are functions of the

axis variable, using a energy equivalence equation, a 6×6 sectional stiffness matrix which connects the overall sectional resultants and the generalized beam strains can be obtained. Subsequently this theory was developed to account for large displacement, initial curvature and twist(Borri and Merlini, 1986). This procedure has been extended to beams made of smart materials by (Ghiringhelli et al., 1997) and later to thermoelastic beams (Ghiringhelli, 1997). In (Mielke, 1988, 1991), the center manifold of an elastic prism, was investigated by adopting Hamiltonian formalism, and the four Jordan chains were identified, which are the basis of de Saint-Venant's solutions. A symplectic method which based on Hamiltonian system was developed in (Zhong et al., 1996). A Hamiltonian matrix is not diagonal, but can be reduced to a Jordan form, and its null eigenvalues generate polynomial solutions. Later this method was also extended to 2D smart beams with piezoelectric patches (Gu et al., 2005). Unlike the former methods following (Giavotto et al., 1983), in (Morandini et al., 2010), the solid beam equation was derived without a-priori separation of nodal displacement into reference section displacement and a wrapping field, and a numerical method was exploited to calculate the generalized eigenvectors corresponding to null eigenvalues of Hamiltonian matrix referring to the second order differential equation hierarchically rather than tightly depend on Hamiltonian matrix. Later the author extended this procedure to smart beams that contains piezoelectric devices (Brillante et al., 2015). Rooting in the symplectic method proposed in (Zhong et al., 1996), a comprehensive framework aiming to solve the de Saint-Venant problem was developed in (Bauchau and Han, 2014; Han and Bauchau, 2015, 2016). In this work, a set of structure preserving transformations using symplectic matrices was adopted, and the Hamiltonian matrix was projected to its subspace relating to null eigenvalues, and this yields a set of linear equations regarding to nodal wrapping and sectional compliance matrix, instead of solving derogatory eigenvalue problems.

Based on the generalized eigenvectors method proposed in (Morandini et al., 2010), this paper develops a general and efficient method for predicting prismatic smart beam cross-section characteristics. The same problems tackled in (Wang and Yu, 2012) are addressed, with the addition of possible thermal loading. The present formulation, however, is not based on the variationally asymptotic method, and naturally accounts for shear deformations. The content is organized as follows: first, the kinematics of the beam problem is described, the multiphysics fields constitutive relationships are presented and the weak form of smart beam are derived without any a-priori assumptions. A numerical solving procedure is adopted subsequently and the cross-section stiffness matrix is derived, then the three dimensional variables recovery formula is derived. At last, some numerical examples are carried out, and the results obtained by present method are compared with results of full three dimensional finite element analysis.

2. Beam cross-section multiphysics field description

Consider a straight beam slice with arbitrary plane cross-section geometry as depicted in Figure 1.

Unit vectors $\boldsymbol{i}^1$, $\boldsymbol{i}^2$ and $\boldsymbol{i}^3$ are aligned with the chosen orthogonal reference system, with $\boldsymbol{i}^3$ parallel to the beam axis and normal to the cross-section. Assume an arbitrary point P on the cross-section with position $\boldsymbol{x} = x\boldsymbol{i}^1 + y\boldsymbol{i}^2$. Let $\boldsymbol{x}'(\boldsymbol{x}, z)$ be the position of P in deformed configuration, so that its displacement is $\boldsymbol{u}(\boldsymbol{x}, z) = \boldsymbol{x}' - \boldsymbol{x}$, and
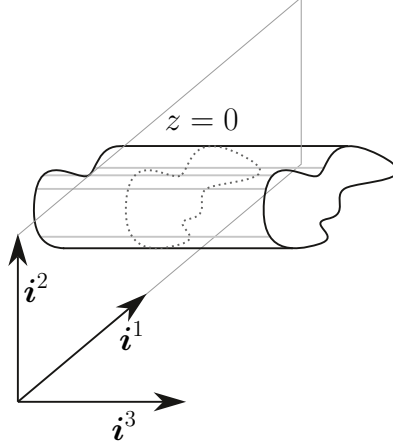
Figure 1.: Beam cross-section.

$\delta \boldsymbol{u} = \delta \boldsymbol{x}'$. The deformation gradient $\boldsymbol{F}$ is defined as

$$\boldsymbol{F} = \mathrm{grad}_S(\boldsymbol{x}') + \boldsymbol{x}'_{,z} \otimes \boldsymbol{i}^3 \tag{1}$$

where $\mathrm{grad}_S(\boldsymbol{x}') = \boldsymbol{x}'_{,x} \otimes \boldsymbol{i}^1 + \boldsymbol{x}'_{,y} \otimes \boldsymbol{i}^2$ and $\boldsymbol{x}'_{,x}$, $\boldsymbol{x}'_{,y}$ and $\boldsymbol{x}'_{,z}$ stand for the partial derivative of $\boldsymbol{x}'$ with respect to the coordinate x, y, z, respectively. The virtual variation of deformation gradient is given by

$$\delta \boldsymbol{F} = \delta\mathrm{grad}_S(\boldsymbol{x}') + \delta\boldsymbol{x}'_{,z} \otimes \boldsymbol{i}^3 \tag{2}$$

Assuming infinitesimal deformation and displacement field, the small strain tensor is defined as

$$\boldsymbol{\epsilon} = \frac{1}{2}(\boldsymbol{F}^T + \boldsymbol{F}) \tag{3}$$

Considering the thermal conduction, the heat flux equilibrium equation is as follows

$$\mathrm{div}(\boldsymbol{\Phi}) = S_T \tag{4}$$

where $\boldsymbol{\Phi}$ is the heat flux vector, and S_T is the heat source per unit of undeformed volume. The variational form of thermal conduction can be formulated as

$$\int_V -\delta\mathrm{grad}(T) \cdot \boldsymbol{\Phi}\mathrm{d}V = \int_A \delta T q_T \mathrm{d}A + \int_{\partial V} \delta T q_{Tc}\mathrm{d}\partial V + \int_V \delta T S_T \mathrm{d}V \tag{5}$$

where T is the temperature and q_T is the heat flux entering the two beam extremities, q_{Tc} is the heat flux entering the beam lateral surface. The heat flux vector $\boldsymbol{\Phi}$ is related to the gradient of the temperature $\mathrm{grad}(T)$ by the well-known Fourier heat conduction law

$$\boldsymbol{\Phi} = -\boldsymbol{K} \cdot \mathrm{grad}(T) \tag{6}$$

where $\boldsymbol{K}$ is the thermal conductivity tensor. The electric field and magnetic field need to be accounted for as well. These two fields are characterized by the electric potential $\boldsymbol{\phi}$ and magnetic potential $\boldsymbol{\psi}$ as

$$\boldsymbol{E} = -\text{grad}(\boldsymbol{\phi}) \tag{7}$$

$$\boldsymbol{H} = -\text{grad}(\boldsymbol{\psi}) \tag{8}$$

where $\boldsymbol{E}$ and $\boldsymbol{H}$ are the electric field intensity and magnetic field strength respectively. The multiphysics fields constitutive law can be expressed as

$$\left\{ \begin{array}{c} \boldsymbol{S} \\ \boldsymbol{D} \\ \boldsymbol{B} \end{array} \right\} = \left[\begin{array}{ccc} \boldsymbol{\Gamma} & -\boldsymbol{d}^{T231} & -\boldsymbol{q}^{T231} \\ \boldsymbol{d} & \boldsymbol{\varepsilon} & \boldsymbol{m} \\ \boldsymbol{q} & \boldsymbol{m}^T & \boldsymbol{\mu} \end{array} \right] \left\{ \begin{array}{c} : \boldsymbol{\epsilon} \\ \cdot \boldsymbol{E} \\ \cdot \boldsymbol{H} \end{array} \right\} + \left\{ \begin{array}{c} -\boldsymbol{\Gamma} : \boldsymbol{\alpha} \\ \boldsymbol{p} \\ \boldsymbol{k} \end{array} \right\} \Delta T \tag{9}$$

where $\boldsymbol{S}$, $\boldsymbol{D}$ and $\boldsymbol{B}$ are the stress tensor, the electric displacement and the magnetic flux, respectively, $\boldsymbol{\Gamma}$ is the elastic tensor, $\boldsymbol{d}$ is the piezoelectric tensor, $\boldsymbol{q}$ is the piezomagnetic tensor, $\boldsymbol{\varepsilon}$ is the dielectric tensor, $\boldsymbol{m}$ is the magneto-electric coupling tensor, $\boldsymbol{\mu}$ is the magnetic permeability tensor, and $\boldsymbol{\alpha}$ is the thermal expansion tensor; finally, $\boldsymbol{p}$ and $\boldsymbol{k}$ are the pyroelectric tensor and pyromagnetic tensor, respectively. The notation $\boldsymbol{d}^{T231}$ stands for the transpose of the third-order tensor $\boldsymbol{d}$ obtained by changing the order of the dyadic bases, so that if tensor $\boldsymbol{d} = d_{ijk}\boldsymbol{i}^i \otimes \boldsymbol{i}^j \otimes \boldsymbol{i}^k$ then $\boldsymbol{d}^{T231} = d_{ijk}\boldsymbol{i}^j \otimes \boldsymbol{i}^k \otimes \boldsymbol{i}^i$.

3. Governing equations

Considering a straight smart beam slice with length L, the internal work can be formulated as

$$\delta \boldsymbol{L}_i = \int_V \delta\boldsymbol{\epsilon} : \boldsymbol{S}\mathrm{d}V + \int_{V_\phi} \delta\boldsymbol{E} \cdot \boldsymbol{D}\mathrm{d}V_\phi + \int_{V_\psi} \delta\boldsymbol{H} \cdot \boldsymbol{B}\mathrm{d}V_\psi - \int_V \delta\text{grad}(T) \cdot \boldsymbol{\Phi}\mathrm{d}V \tag{10}$$

where V is the beam volume, V_ϕ is the volume of piezoelectric regions, and V_ψ is the volume of piezomagntic regions. Substituting equation (2, 3) into the first term of equation (10), and integrating by part, leads to

$$\begin{aligned}
\int_V \delta\boldsymbol{\epsilon} : \boldsymbol{S}dV &= \int_L \int_A \delta\text{grad}_S(\boldsymbol{x}') : \boldsymbol{S}\mathrm{d}A\mathrm{d}z + \int_L \int_A \delta\boldsymbol{x}'_{,z} \otimes \boldsymbol{i}^3 : \boldsymbol{S}\mathrm{d}A\mathrm{d}z \\
&= \int_L \int_A \delta\text{grad}_S(\boldsymbol{x}') : \boldsymbol{S}\mathrm{d}A\mathrm{d}z + \int_L \int_A \delta\boldsymbol{x}'_{,z} \cdot \boldsymbol{S} \cdot \boldsymbol{n}\mathrm{d}A\mathrm{d}z \\
&= \int_L \int_A \delta\text{grad}_S(\boldsymbol{x}') : \boldsymbol{S}\mathrm{d}A\mathrm{d}z + \int_A \delta\boldsymbol{x}' \cdot \boldsymbol{S} \cdot \boldsymbol{n}\mathrm{d}A \Big|_0^L \\
&\quad - \int_L \int_A \delta\boldsymbol{x}' \cdot \boldsymbol{S}_{,z} \cdot \boldsymbol{n}\mathrm{d}A\mathrm{d}z
\end{aligned} \tag{11}$$

The same procedure can be applied to the rest terms of equation (10). The external work can be expressed as

5

$$\delta L_e = \int_A \delta \boldsymbol{x}(L) \cdot \boldsymbol{f}(L) \mathrm{d}A - \int_A \delta \boldsymbol{x}(0) \cdot \boldsymbol{f}(0) \mathrm{d}A$$

$$+ \int_{A_\phi} \delta \phi(L) q_\phi(L) \mathrm{d}A_\phi - \int_{A_\phi} \delta \phi(0) q_\phi(0) \mathrm{d}A_\phi + \int_{\partial V_\phi} \delta \phi q_{\phi c} \mathrm{d}\partial V_\phi$$

$$+ \int_{A_\psi} \delta \psi(L) q_\psi(L) \mathrm{d}A_\psi - \int_{A_\psi} \delta \psi(0) q_\psi(0) \mathrm{d}A_\psi + \int_{\partial V_\psi} \delta \psi q_{\psi c} \mathrm{d}\partial V_\psi$$

$$+ \int_A \delta T(L) q_T(L) \mathrm{d}A - \int_A \delta T(0) q_T(0) \mathrm{d}A + \int_{\partial V} \delta T q_{Tc} \mathrm{d}\partial V \qquad (12)$$

$$+ \int_V \delta T S_T \mathrm{d}V.$$

where the following prescribed quantities are defined as $\boldsymbol{f}$ the end surface traction, q_ϕ the end surface charge, q_ψ the end surface magnetic flux, q_T the surface heat flux, $q_{\phi c}$ the lateral surface charge, $q_{\psi c}$ the lateral surface magnetic flux, q_{Tc} the lateral surface heat flux, S_T the heat source (Allik and Hughes, 1970). A_ϕ, A_ψ are the areas of the piezoelectric regions and piezomagnetic regions over the cross-section respectively. Internal heat source is not accounted for.

According to the virtual work principle $\delta L_i = \delta L_e$, and accounting for the arbitrariness of virtual filed variables, yields the following set of variational equations:

$$-\int_L \int_A \delta \boldsymbol{x}' \cdot \boldsymbol{S}_{,z} \cdot \boldsymbol{n} \mathrm{d}A \mathrm{d}z + \int_L \int_A \delta \mathrm{grad}_S(\boldsymbol{x}') : \boldsymbol{S} \mathrm{d}A \mathrm{d}z \qquad (13)$$

$$+ \left[\int_A \delta \boldsymbol{x}' \cdot (\boldsymbol{S} \cdot \boldsymbol{n} - \boldsymbol{f}) \mathrm{d}A \right]_L - \left[\int_A \delta \boldsymbol{x}' \cdot (\boldsymbol{S} \cdot \boldsymbol{n} - \boldsymbol{f}) dA \right]_0 = 0;$$

$$-\int_L \int_{A_\phi} \delta \mathrm{grad}_S(\phi) \cdot \boldsymbol{D} \mathrm{d}A_\phi \mathrm{d}z + \int_L \int_{A_\phi} \delta \phi \boldsymbol{D}_{,z} \cdot \boldsymbol{n} \mathrm{d}A_\phi \mathrm{d}z \qquad (14)$$

$$-\left[\int_{A_\phi} \delta \phi (\boldsymbol{D} \cdot \boldsymbol{n} - q_\phi) \mathrm{d}A_\phi \right]_L + \left[\int_{A_\phi} \delta \phi (\boldsymbol{D} \cdot \boldsymbol{n} - q_\phi) \mathrm{d}A_\phi \right]_0 = \int_{\partial V_\phi} \delta \phi q_{\phi c} \mathrm{d}\partial V_\phi;$$

$$-\int_L \int_{A_\psi} \delta \mathrm{grad}_S(\psi) \cdot \boldsymbol{B} \mathrm{d}A_\psi \mathrm{d}z + \int_L \int_{A_\psi} \delta \psi \boldsymbol{B}_{,z} \cdot \boldsymbol{n} \mathrm{d}A_\psi \mathrm{d}z \qquad (15)$$

$$-\left[\int_{A_\psi} \delta \psi (\boldsymbol{B} \cdot \boldsymbol{n} - q_\psi) \mathrm{d}A_\psi \right]_L + \left[\int_{A_\psi} \delta \psi (\boldsymbol{B} \cdot \boldsymbol{n} - q_\psi) \mathrm{d}A_\psi \right]_0 = \int_{\partial V_\psi} \delta \psi q_{\psi c} \mathrm{d}\partial V_\psi;$$

$$-\int_L \int_A \delta \mathrm{grad}_S(T) \cdot \boldsymbol{\Phi} \mathrm{d}A \mathrm{d}z + \int_L \int_A \delta T \boldsymbol{\Phi}_{,z} \cdot \boldsymbol{n} \mathrm{d}A \mathrm{d}z \qquad (16)$$

$$-\left[\int_A \delta T (\boldsymbol{\Phi} \cdot \boldsymbol{n} - q_T) \mathrm{d}A \right]_L + \left[\int_A \delta T (\boldsymbol{\Phi} \cdot \boldsymbol{n} - q_T) \mathrm{d}A \right]_0 = \int_{\partial V} \delta T q_{Tc} \mathrm{d}\partial V.$$

The first two terms in the left hand of equation (13-16) lead to the equilibrium equation of each field, while the last two terms represent the natural boundary conditions at

two ends of the beam. The equilibrium equation can be reduced to a set of second order ordinary differential equations by using the semi-analytical method proposed in (Giavotto et al., 1983). The displacement, electric potential, magnetic potential and temperature fields can be approximated by a shape function depending on the cross-section geometry parameters and nodal field components along the beam axis.

$$\boldsymbol{u}(\boldsymbol{x}, z) = \sum_i N_{i(u)}(\boldsymbol{x})\boldsymbol{u}_i(z) \tag{17}$$

$$\phi(\boldsymbol{x}, z) = \sum_i N_{i(\phi)}(\boldsymbol{x})\phi_i(z) \tag{18}$$

$$\psi(\boldsymbol{x}, z) = \sum_i N_{i(\psi)}(\boldsymbol{x})\psi_i(z) \tag{19}$$

$$T(\boldsymbol{x}, z) = \sum_i N_{i(T)}(\boldsymbol{x})T_i(z) \tag{20}$$

Introducing the Fourier law equation (6) together with the linear constitutive law equation (9) into equation (13-16), and approximating the problem by means of equation (17-20) yields the following set of differential equations

$$
\begin{bmatrix}
\boldsymbol{M}_{uu} & \boldsymbol{M}_{u\phi} & \boldsymbol{M}_{u\psi} & \boldsymbol{0} \\
\boldsymbol{M}_{u\phi}^T & -\boldsymbol{M}_{\phi\phi} & -\boldsymbol{M}_{\phi\psi} & \boldsymbol{0} \\
\boldsymbol{M}_{u\psi}^T & -\boldsymbol{M}_{\psi\phi}^T & -\boldsymbol{M}_{\psi\psi} & \boldsymbol{0} \\
\boldsymbol{0} & \boldsymbol{0} & \boldsymbol{0} & -\boldsymbol{M}_{TT}
\end{bmatrix}
\begin{Bmatrix}
\hat{\boldsymbol{u}}_{,zz} \\
\hat{\boldsymbol{\phi}}_{,zz} \\
\hat{\boldsymbol{\psi}}_{,zz} \\
\hat{\boldsymbol{T}}_{,zz}
\end{Bmatrix}
$$

$$
- \begin{bmatrix}
\boldsymbol{C}_{uu} - \boldsymbol{C}_{uu}^T & \boldsymbol{C}_{u\phi} - \boldsymbol{C}_{\phi u}^T & \boldsymbol{C}_{u\psi} - \boldsymbol{C}_{\psi u}^T & \boldsymbol{C}_{uT} \\
\boldsymbol{C}_{\phi u} - \boldsymbol{C}_{u\phi}^T & \boldsymbol{C}_{\phi\phi}^T - \boldsymbol{C}_{\phi\phi} & \boldsymbol{C}_{\psi\phi}^T - \boldsymbol{C}_{\phi\psi} & -\boldsymbol{C}_{\phi T} \\
\boldsymbol{C}_{\psi u} - \boldsymbol{C}_{u\psi}^T & \boldsymbol{C}_{\phi\psi}^T - \boldsymbol{C}_{\psi\phi} & \boldsymbol{C}_{\psi\psi}^T - \boldsymbol{C}_{\psi\psi} & -\boldsymbol{C}_{\psi T} \\
\boldsymbol{0} & \boldsymbol{0} & \boldsymbol{0} & \boldsymbol{C}_{TT}^T - \boldsymbol{C}_{TT}
\end{bmatrix}
\begin{Bmatrix}
\hat{\boldsymbol{u}}_{,z} \\
\hat{\boldsymbol{\phi}}_{,z} \\
\hat{\boldsymbol{\psi}}_{,z} \\
\hat{\boldsymbol{T}}_{,z}
\end{Bmatrix}
$$

$$
- \begin{bmatrix}
\boldsymbol{E}_{uu}^T & \boldsymbol{E}_{u\phi} & \boldsymbol{E}_{u\psi} & -\boldsymbol{E}_{uT} \\
\boldsymbol{E}_{u\phi}^T & -\boldsymbol{E}_{\phi\phi} & -\boldsymbol{E}_{\phi\psi} & \boldsymbol{E}_{\phi T} \\
\boldsymbol{E}_{u\psi}^T & -\boldsymbol{E}_{\psi\phi}^T & -\boldsymbol{E}_{\psi\psi} & \boldsymbol{E}_{\psi T} \\
\boldsymbol{0} & \boldsymbol{0} & \boldsymbol{0} & -\boldsymbol{E}_{TT}
\end{bmatrix}
\begin{Bmatrix}
\hat{\boldsymbol{u}} \\
\hat{\boldsymbol{\phi}} \\
\hat{\boldsymbol{\psi}} \\
\hat{\boldsymbol{T}}
\end{Bmatrix}
= \begin{Bmatrix}
\boldsymbol{0} \\
\hat{\boldsymbol{P}}_\phi \\
\hat{\boldsymbol{P}}_\psi \\
\hat{\boldsymbol{P}}_T
\end{Bmatrix}
\tag{21}
$$

where vectors $\hat{\boldsymbol{u}}$, $\hat{\boldsymbol{\phi}}$, $\hat{\boldsymbol{\psi}}$ and $\hat{\boldsymbol{T}}$ stand for the finite-dimensional vectors of nodal unknowns obtained by stacking the different $\boldsymbol{u}_i$, ϕ_i ψ_i and T_i of the whole mesh, and $\hat{\boldsymbol{P}}_\phi$, $\hat{\boldsymbol{P}}_\psi$ and $\hat{\boldsymbol{P}}_T$ stand for the discrete right hand side vectors obtained after applying equation (17-20) to equation (13-16). The matrices defined in equation (21) are given in A. Equation (21) can be recast as a more compact form

$$
\boldsymbol{M}
\begin{Bmatrix}
\hat{\boldsymbol{u}}_{,zz} \\
\hat{\boldsymbol{\phi}}_{,zz} \\
\hat{\boldsymbol{\psi}}_{,zz} \\
\hat{\boldsymbol{T}}_{,zz}
\end{Bmatrix}
- \boldsymbol{H}
\begin{Bmatrix}
\hat{\boldsymbol{u}}_{,z} \\
\hat{\boldsymbol{\phi}}_{,z} \\
\hat{\boldsymbol{\psi}}_{,z} \\
\hat{\boldsymbol{T}}_{,z}
\end{Bmatrix}
- \boldsymbol{E}
\begin{Bmatrix}
\hat{\boldsymbol{u}} \\
\hat{\boldsymbol{\phi}} \\
\hat{\boldsymbol{\psi}} \\
\hat{\boldsymbol{T}}
\end{Bmatrix}
= \begin{Bmatrix}
\boldsymbol{0} \\
\hat{\boldsymbol{P}}_\phi \\
\hat{\boldsymbol{P}}_\psi \\
\hat{\boldsymbol{P}}_T
\end{Bmatrix}
\tag{22}
$$

Matrix $\boldsymbol{E}_{uu}$ is four times singular, because of the four rigid motions of the cross-section, i.e. three the rigid translations and the rotation around the beam axis. These rigid motions create no strains and can be constrained by using four Lagrange multipliers to force the section average displacements to be null.

$$\int_A \boldsymbol{u}\mathrm{d}A = \boldsymbol{0} \tag{23}$$

$$\int_A \boldsymbol{x} \times \boldsymbol{u}\mathrm{d}A = \boldsymbol{0} \tag{24}$$

As for $\boldsymbol{E}_{\phi\phi}$ and $\boldsymbol{E}_{\psi\psi}$, they are singular as many times as the number of the independent piezoelectric and piezomagnetic regions since the electric or magnetic potential of each independent region is defined up to a constant. Electrodes are not modeled explicitly, rather, they are accounted for by applying equal potential boundary conditions on the corresponding nodes. By applying Dirichlet boundary conditions on each electrode region, $\boldsymbol{E}_{\phi\phi}$ and $\boldsymbol{E}_{\psi\psi}$ are brought to full rank. The same case is suit for $\boldsymbol{E}_{TT}$.

4. Beam cross-section characteristics

For the smart beam slice, the internal work can be formulated as

$$\delta L_i = \int_V \delta\boldsymbol{\epsilon} : \boldsymbol{S}\mathrm{d}V + \int_{V_p} \delta\boldsymbol{E} \cdot \boldsymbol{D}\mathrm{d}V_p + \int_{V_m} \delta\boldsymbol{H} \cdot \boldsymbol{B}\mathrm{d}V_m - \int_V \delta\mathrm{grad}(T) \cdot \boldsymbol{\Phi}\mathrm{d}V$$

$$= \int_L \left\{ \begin{array}{c} \delta\hat{\boldsymbol{u}}_{,z} \\ \delta\hat{\boldsymbol{\phi}}_{,z} \\ \delta\hat{\boldsymbol{\psi}}_{,z} \\ \delta\hat{\boldsymbol{T}}_{,z} \\ \delta\hat{\boldsymbol{u}} \\ \delta\hat{\boldsymbol{\phi}} \\ \delta\hat{\boldsymbol{\psi}} \\ \delta\hat{\boldsymbol{T}} \end{array} \right\}^T \left[\begin{array}{cccccccc} \boldsymbol{M}_{uu} & \boldsymbol{M}_{u\phi} & \boldsymbol{M}_{u\psi} & \boldsymbol{0} & \boldsymbol{C}_{uu}^T & \boldsymbol{C}_{\phi u}^T & \boldsymbol{C}_{\psi u}^T & -\boldsymbol{C}_{Tu}^T \\ -\boldsymbol{M}_{u\phi}^T & \boldsymbol{M}_{\phi\phi} & \boldsymbol{M}_{\phi\psi} & \boldsymbol{0} & -\boldsymbol{C}_{u\phi}^T & \boldsymbol{C}_{\phi\phi}^T & \boldsymbol{C}_{\psi\phi}^T & -\boldsymbol{C}_{T\phi}^T \\ -\boldsymbol{M}_{u\psi}^T & \boldsymbol{M}_{\psi\phi}^T & \boldsymbol{M}_{\psi\psi} & \boldsymbol{0} & -\boldsymbol{C}_{u\psi}^T & \boldsymbol{C}_{\phi\psi}^T & \boldsymbol{C}_{\psi\psi}^T & -\boldsymbol{C}_{T\psi}^T \\ \boldsymbol{0} & \boldsymbol{0} & \boldsymbol{0} & \boldsymbol{M}_{TT} & \boldsymbol{0} & \boldsymbol{0} & \boldsymbol{0} & \boldsymbol{C}_{TT}^T \\ \boldsymbol{C}_{uu} & \boldsymbol{C}_{u\phi} & \boldsymbol{C}_{u\psi} & \boldsymbol{0} & \boldsymbol{E}_{uu}^T & \boldsymbol{E}_{u\phi} & \boldsymbol{E}_{u\psi} & -\boldsymbol{E}_{uT} \\ -\boldsymbol{C}_{\phi u} & \boldsymbol{C}_{\phi\phi} & \boldsymbol{C}_{\phi\psi} & \boldsymbol{0} & -\boldsymbol{E}_{u\phi}^T & \boldsymbol{E}_{\phi\phi} & \boldsymbol{E}_{\phi\psi} & \boldsymbol{E}_{\phi T} \\ -\boldsymbol{C}_{\psi u} & \boldsymbol{C}_{\psi\phi} & \boldsymbol{C}_{\psi\psi} & \boldsymbol{0} & -\boldsymbol{E}_{u\psi}^T & \boldsymbol{E}_{\psi\phi}^T & \boldsymbol{E}_{\psi\psi} & \boldsymbol{E}_{\psi T} \\ \boldsymbol{0} & \boldsymbol{0} & \boldsymbol{0} & \boldsymbol{C}_{TT} & \boldsymbol{0} & \boldsymbol{0} & \boldsymbol{0} & \boldsymbol{E}_{TT} \end{array} \right] \left\{ \begin{array}{c} \hat{\boldsymbol{u}}_{,z} \\ \hat{\boldsymbol{\phi}}_{,z} \\ \hat{\boldsymbol{\psi}}_{,z} \\ \hat{\boldsymbol{T}}_{,z} \\ \hat{\boldsymbol{u}} \\ \hat{\boldsymbol{\phi}} \\ \hat{\boldsymbol{\psi}} \\ \hat{\boldsymbol{T}} \end{array} \right\} \mathrm{d}z$$

$$= \int_L \delta\hat{\boldsymbol{q}}^T \cdot \boldsymbol{K}_{FEM} \cdot \hat{\boldsymbol{q}}\mathrm{d}z \tag{25}$$

Where $\hat{\boldsymbol{q}} = \left\{ \begin{array}{cccccccc} \hat{\boldsymbol{u}}_{,z} & \hat{\boldsymbol{\phi}}_{,z} & \hat{\boldsymbol{\psi}}_{,z} & \hat{\boldsymbol{T}}_{,z} & \hat{\boldsymbol{u}} & \hat{\boldsymbol{\phi}} & \hat{\boldsymbol{\psi}} & \hat{\boldsymbol{T}} \end{array} \right\}^T$ is the nodal state variable, a $1 \times 2N$ vector, $N = 6n$ denotes the number of degree of freedoms (DOFs), and n is the nodes number of the whole mesh. In this paper, each node has 6 DOFs including 3 displacement components, the electric potential, the magnetic potential and the temperature, no matter what kind of materials the node is corresponding to. Matrix $\boldsymbol{K}_{FEM}$ is the global stiffness matrix. In order to build a one dimension beam model, and following the procedure in (Morandini et al., 2010), the structural state variables $\hat{\boldsymbol{u}}_{,z}$ and $\hat{\boldsymbol{u}}$ of the three dimensional problem are projected onto the vector space defined by the so-called de Saint-Venant's beam solutions. By doing so the nodal finite

element displacement $\hat{\boldsymbol{u}}$ is assumed to be function of the six beam generalized deformation parameters $\boldsymbol{\varphi}$ that are energetically conjugated to the six average sectional stress resultants $\boldsymbol{\vartheta}$. The nodal potential $\hat{\boldsymbol{\phi}}$, $\hat{\boldsymbol{\psi}}$, and $\hat{\boldsymbol{T}}$ can be determined, up to a constant, if the potential differences between all the electrodes are known. Thus the number of DOFs associated with electric potential, magnetic potential and temperature can be reduced to $N_c = N_{\phi_c} + N_{\psi_c} + N_{T_c}$, with N_{ϕ_c}, N_{ψ_c} and N_{T_c} the number of independent regions corresponding to the electric, magnetic and thermal field, respectively. The overall sectional electric charge $\boldsymbol{d}_c$ is energetically conjugated the electrodes potential difference $\boldsymbol{\phi}_c$, the sectional magnetic flux $\boldsymbol{h}_c$ with the magnetic potential $\boldsymbol{\psi}_c$, and the sectional heat flux $\boldsymbol{\Phi}_c$ with the temperature $\boldsymbol{T}_c$. The generalized coordinates for the multiphysics beam can be expanded to $\boldsymbol{\varphi}$, $\boldsymbol{\phi}_c$, $\boldsymbol{\psi}_c$, $\boldsymbol{T}_c$. Here $\boldsymbol{T}_c$ is the imposed temperature difference from reference temperature. The projection results into

$$
\hat{\boldsymbol{q}} = \begin{bmatrix} \boldsymbol{Q}_\varphi & \boldsymbol{Q}_\phi & \boldsymbol{Q}_\psi & \boldsymbol{Q}_T \end{bmatrix} \begin{Bmatrix} \boldsymbol{\varphi} \\ \boldsymbol{\phi}_c \\ \boldsymbol{\psi}_c \\ \boldsymbol{T}_c \end{Bmatrix} \tag{26}
$$

where $\boldsymbol{Q}_\varphi$, of size $2N \times 6$, is computed from the de Saint-Venant's solutions, $\boldsymbol{Q}_\phi$ is a $2N \times N_{\phi_c}$ matrix, $\boldsymbol{Q}_\psi$ is a $2N \times N_{\psi_c}$ matrix, and $\boldsymbol{Q}_T$ is a $2N \times N_{T_c}$ matrix. The matrix $\boldsymbol{Q}_\phi$ characterizes the smart beam behaviors when unit electric potential is applied on each electrode, while keeping $\boldsymbol{\psi}_c$ and $\boldsymbol{T}_c$ null, describes a particular solution of equation (21). Matrices $\boldsymbol{Q}_\psi$ and $\boldsymbol{Q}_T$ are computed in a similar way by imposing unit magnetic potentials or boundary temperatures, respectively. Accordingly, the virtual internal work can be expressed by

$$
\delta L_i = \int_L \delta \begin{Bmatrix} \boldsymbol{\varphi} \\ \boldsymbol{\phi}_c \\ \boldsymbol{\psi}_c \\ \boldsymbol{T}_c \end{Bmatrix}^T \begin{bmatrix} \boldsymbol{Q}_\varphi^T \\ \boldsymbol{Q}_\phi^T \\ \boldsymbol{Q}_\psi^T \\ \boldsymbol{Q}_T^T \end{bmatrix} \boldsymbol{K}_{FEM} \begin{bmatrix} \boldsymbol{Q}_\varphi & \boldsymbol{Q}_\phi & \boldsymbol{Q}_\psi & \boldsymbol{Q}_T \end{bmatrix} \begin{Bmatrix} \boldsymbol{\varphi} \\ \boldsymbol{\phi}_c \\ \boldsymbol{\psi}_c \\ \boldsymbol{T}_c \end{Bmatrix} \mathrm{d}z \tag{27}
$$

On the other hand, For a beam with linear constitutive law as depicted in equation (9), its generalized sectional resultants and generalized deformations have linear relationship,

$$
\begin{Bmatrix} \boldsymbol{\vartheta} \\ \boldsymbol{d}_c \\ \boldsymbol{h}_c \\ \boldsymbol{\Phi}_c \end{Bmatrix} = \boldsymbol{K}_{BEAM} \begin{Bmatrix} \boldsymbol{\varphi} \\ \boldsymbol{\phi}_c \\ \boldsymbol{\psi}_c \\ \boldsymbol{T}_c \end{Bmatrix} = \begin{bmatrix} \boldsymbol{K}_{\varphi\varphi} & \boldsymbol{K}_{\varphi\phi} & \boldsymbol{K}_{\varphi\psi} & \boldsymbol{K}_{\varphi T} \\ \boldsymbol{K}_{\phi\varphi} & \boldsymbol{K}_{\phi\phi} & \boldsymbol{K}_{\phi\psi} & \boldsymbol{K}_{\phi T} \\ \boldsymbol{K}_{\psi\varphi} & \boldsymbol{K}_{\psi\phi} & \boldsymbol{K}_{\psi\psi} & \boldsymbol{K}_{\psi T} \\ \boldsymbol{K}_{T\varphi} & \boldsymbol{K}_{T\phi} & \boldsymbol{K}_{T\psi} & \boldsymbol{K}_{TT} \end{bmatrix} \begin{Bmatrix} \boldsymbol{\varphi} \\ \boldsymbol{\phi}_c \\ \boldsymbol{\psi}_c \\ \boldsymbol{T}_c \end{Bmatrix} \tag{28}
$$

After substituting equation(28) into equation (27) and equating the two expressions leads to

$$
\begin{aligned}
\delta \boldsymbol{L}_i &= \int_L \delta \left\{ \begin{array}{c} \boldsymbol{\varphi} \\ \boldsymbol{\phi}_c \\ \boldsymbol{\psi}_c \\ \boldsymbol{T}_c \end{array} \right\} \left[\begin{array}{c} \boldsymbol{Q}_\varphi^T \\ \boldsymbol{Q}_\phi^T \\ \boldsymbol{Q}_\psi^T \\ \boldsymbol{Q}_T^T \end{array} \right] \boldsymbol{K}_{FEM} \left[\begin{array}{cccc} \boldsymbol{Q}_\varphi & \boldsymbol{Q}_\phi & \boldsymbol{Q}_\psi & \boldsymbol{Q}_T \end{array} \right] \left\{ \begin{array}{c} \boldsymbol{\varphi} \\ \boldsymbol{\phi}_c \\ \boldsymbol{\psi}_c \\ \boldsymbol{T}_c \end{array} \right\} \mathrm{d}z \\
&= \int_L \delta \left\{ \begin{array}{c} \boldsymbol{\varphi} \\ \boldsymbol{\phi}_c \\ \boldsymbol{\psi}_c \\ \boldsymbol{T}_c \end{array} \right\}^T \left\{ \begin{array}{c} \boldsymbol{\vartheta} \\ \boldsymbol{d}_c \\ \boldsymbol{h}_c \\ \boldsymbol{\Phi}_c \end{array} \right\} \mathrm{d}z \\
&= \int_L \delta \left\{ \begin{array}{c} \boldsymbol{\varphi} \\ \boldsymbol{\phi}_c \\ \boldsymbol{\psi}_c \\ \boldsymbol{T}_c \end{array} \right\}^T \boldsymbol{K}_{BEAM} \left\{ \begin{array}{c} \boldsymbol{\varphi} \\ \boldsymbol{\phi}_c \\ \boldsymbol{\psi}_c \\ \boldsymbol{T}_c \end{array} \right\} \mathrm{d}z
\end{aligned} \tag{29}
$$

so that

$$
\left\{ \begin{array}{c} \boldsymbol{\vartheta} \\ \boldsymbol{d}_c \\ \boldsymbol{h}_c \\ \boldsymbol{\Phi}_c \end{array} \right\} = \left[\begin{array}{c} \boldsymbol{Q}_\varphi^T \\ \boldsymbol{Q}_\phi^T \\ \boldsymbol{Q}_\psi^T \\ \boldsymbol{Q}_T^T \end{array} \right] \boldsymbol{K}_{FEM} \left[\begin{array}{cccc} \boldsymbol{Q}_\varphi & \boldsymbol{Q}_\phi & \boldsymbol{Q}_\psi & \boldsymbol{Q}_T \end{array} \right] \left\{ \begin{array}{c} \boldsymbol{\varphi} \\ \boldsymbol{\phi}_c \\ \boldsymbol{\psi}_c \\ \boldsymbol{T}_c \end{array} \right\} \tag{30}
$$

$$
\boldsymbol{K}_{BEAM} = \left[\begin{array}{cccc} \boldsymbol{Q}_\varphi & \boldsymbol{Q}_\phi & \boldsymbol{Q}_\psi & \boldsymbol{Q}_T \end{array} \right]^T \boldsymbol{K}_{FEM} \left[\begin{array}{cccc} \boldsymbol{Q}_\varphi & \boldsymbol{Q}_\phi & \boldsymbol{Q}_\psi & \boldsymbol{Q}_T \end{array} \right] \tag{31}
$$

Section 5 details the numerical procedure used to compute the projection matrices $\boldsymbol{Q}_\varphi$, $\boldsymbol{Q}_\phi$, $\boldsymbol{Q}_\psi$ and $\boldsymbol{Q}_T$.

5. Solution procedure

Equation (22) can be rearranged into a set of first order ordinary differential equations

$$
\left[\begin{array}{cc} \boldsymbol{M} & \boldsymbol{0} \\ \boldsymbol{0} & \boldsymbol{I}_{N \times N} \end{array} \right] \hat{\boldsymbol{q}}_{,z} - \left[\begin{array}{cc} \boldsymbol{H} & \boldsymbol{E} \\ \boldsymbol{I}_{N \times N} & \boldsymbol{0} \end{array} \right] \hat{\boldsymbol{q}} = \left\{ \begin{array}{c} \boldsymbol{W} \\ \boldsymbol{0} \end{array} \right\} \tag{32}
$$

or, more concisely,

$$
\boldsymbol{B} \hat{\boldsymbol{q}}_{,z} = \boldsymbol{A} \hat{\boldsymbol{q}} + \hat{\boldsymbol{W}} \tag{33}
$$

The solution of the non-homogeneous equation (33) is the sum of the homogeneous solution and particular solutions.

5.1. *Homogeneous solution*

The homogeneous solution can be obtained by short-circuiting all the electrodes, such that no electric and magnetic fields exists within the structural domain, and setting a constant temperature field, $\boldsymbol{T}_c = \boldsymbol{0}$, over the whole beam. Thus equation (33) can be reduced to a homogeneous equation which only contains displacement field $\hat{\boldsymbol{u}}$.

$$\tilde{\boldsymbol{q}}_{,z} = \tilde{\boldsymbol{B}}^{-1}\tilde{\boldsymbol{A}}\tilde{\boldsymbol{q}} \tag{34}$$

Where $\tilde{\boldsymbol{q}} = \left\{\begin{array}{cc} \hat{\boldsymbol{u}}_{,z} & \hat{\boldsymbol{u}} \end{array}\right\}$, $\tilde{\boldsymbol{A}} = \left[\begin{array}{cc} \tilde{\boldsymbol{H}} & \tilde{\boldsymbol{E}} \\ \boldsymbol{0} & \boldsymbol{I}_{3n\times 3n} \end{array}\right]$, $\tilde{\boldsymbol{B}} = \left[\begin{array}{cc} \tilde{\boldsymbol{M}} & \boldsymbol{0} \\ \boldsymbol{0} & \boldsymbol{I}_{3n\times 3n} \end{array}\right]$, and $\tilde{\boldsymbol{M}} = \boldsymbol{M}_{uu}$, $\tilde{\boldsymbol{H}} = \boldsymbol{H}_{uu}$, $\tilde{\boldsymbol{E}} = \boldsymbol{E}_{uu}$. The solution procedure of equation (32) has been discussed in (Morandini et al., 2010), see also (Mielke, 1988, 1991) for a more theoretical presentation. Equation (34) is known to have 12 null eigenvalues and $n - 12$ non-zero eigenvalues which show up in conjugated pairs. Matrix $\tilde{\boldsymbol{B}}^{-1}\tilde{\boldsymbol{A}}$ cannot be diagonalized, but can be reduced to a Jordan form. In other words, it is possible to find a coordinate transformation $\boldsymbol{X}$, such that $\boldsymbol{X}^{-1}\tilde{\boldsymbol{B}}^{-1}\tilde{\boldsymbol{A}}\boldsymbol{X} = \boldsymbol{J}$ is a Jordan matrix, and the solution of equation (34) can be written as

$$\tilde{\boldsymbol{q}} = \boldsymbol{X}e^{\boldsymbol{J}z}\boldsymbol{X}^{-1}\tilde{\boldsymbol{q}}_0. \tag{35}$$

Since $e^{\boldsymbol{J}z}$ has the same structure of the Jordan matrix $\boldsymbol{J}$, for a 4-th order Jordan block $\boldsymbol{J}_i(\lambda_k)$ of $\boldsymbol{J}$ corresponding to eigenvalue λ_k, $e^{\boldsymbol{J}_i(\lambda_k)z}$ equals to

$$e^{\boldsymbol{J}_i(\lambda_k)z} = e^{\lambda_k}\left[\begin{array}{cccc} 1 & z & z^2/2 & z^3/3! \\ 0 & 1 & z & z^2/2 \\ 0 & 0 & 1 & z \\ 0 & 0 & 0 & 1 \end{array}\right]. \tag{36}$$

The non-zero eigenvalues $\lambda_k \neq 0$ generate exponential solutions, called "extremity solutions" by (Giavotto et al., 1983), that are rapidly decaying from beam extremities and can thus often be discarded in engineering applications. As for the null eigenvalues $\lambda_k = 0$,

$$\tilde{\boldsymbol{q}} = \boldsymbol{X}\left[\begin{array}{cccc} 1 & z & z^2/2 & z^3/3! \\ 0 & 1 & z & z^2/2 \\ 0 & 0 & 1 & z \\ 0 & 0 & 0 & 1 \end{array}\right]\boldsymbol{X}^{-1}\tilde{\boldsymbol{q}}_0, \tag{37}$$

showing that the null eigenvalues correspond to a set of polynomial solutions of equation (34), often dubbed "central solutions". The polynomial solutions do not decay along axis, and are exactly what we are looking for. They can be computed starting from $\tilde{\boldsymbol{A}}\tilde{\boldsymbol{q}}_0 = \boldsymbol{0}$, and then computing the second term from $\tilde{\boldsymbol{A}}\tilde{\boldsymbol{q}}_1 = \tilde{\boldsymbol{B}}\tilde{\boldsymbol{q}}_0$ subsequently. It is however more meaningful, from a physical point of view, to determine eigenvectors starting from equation (22), so that $\tilde{\boldsymbol{E}}\tilde{\boldsymbol{d}}_0 = 0$. The null-space of $\tilde{\boldsymbol{E}}$, already discussed above, is composed by four global rigid motion of the cross-section, i.e. the rigid translations along the three axis and the rigid rotation around the $\boldsymbol{i}^3$ axis. Starting from

11

these four rigid motion, it is possible to compute four Jordan chains, for a total of 12 eigenvectors. For each Jordan chain, the eigenvectors can be calculated recursively as follows

$$\tilde{\boldsymbol{E}}\tilde{\boldsymbol{d}}_0 = 0 \tag{38}$$

$$\tilde{\boldsymbol{E}}\tilde{\boldsymbol{d}}_1 = -\tilde{\boldsymbol{H}}\tilde{\boldsymbol{d}}_0 \tag{39}$$

$$\tilde{\boldsymbol{E}}\tilde{\boldsymbol{d}}_i = -\tilde{\boldsymbol{H}}\tilde{\boldsymbol{d}}_{i-1} + \tilde{\boldsymbol{M}}\tilde{\boldsymbol{d}}_{i-2} \tag{40}$$

The eigenvectors corresponding to rigid body motion modes are given by

$$
\begin{aligned}
\tilde{\boldsymbol{d}}_0^{axis} &= \begin{bmatrix} \boldsymbol{0} & \boldsymbol{0} & \boldsymbol{I} \end{bmatrix}^T; \\
\tilde{\boldsymbol{d}}_0^{torsion} &= \begin{bmatrix} -\boldsymbol{Y} & \boldsymbol{X} & \boldsymbol{0} \end{bmatrix}^T; \\
\tilde{\boldsymbol{d}}_0^{bend1} &= \begin{bmatrix} \boldsymbol{I} & \boldsymbol{0} & \boldsymbol{0} \end{bmatrix}^T, \qquad \tilde{\boldsymbol{d}}_1^{bend1} = \begin{bmatrix} \boldsymbol{0} & \boldsymbol{0} & -\boldsymbol{Y} \end{bmatrix}^T; \\
\tilde{\boldsymbol{d}}_0^{bend2} &= \begin{bmatrix} \boldsymbol{0} & \boldsymbol{I} & \boldsymbol{0} \end{bmatrix}^T, \qquad \tilde{\boldsymbol{d}}_1^{bend2} = \begin{bmatrix} \boldsymbol{0} & \boldsymbol{0} & -\boldsymbol{X} \end{bmatrix}^T;
\end{aligned}
\tag{41}
$$

where column vectors $\boldsymbol{I}$, $\boldsymbol{X}$, $\boldsymbol{Y}$ are $1 \times n$ vectors, which store unit, x and y-coordinates of nodes on the whole mesh respectively. The first two chains are both composed by two eigenvectors. The first chain is originated from the rigid translation mode along the beam axis, $\tilde{\boldsymbol{d}}_0^{axis}$, and its linear part $\tilde{\boldsymbol{d}}_1^{axis}$ is generated by a constant extension mode along axis $\boldsymbol{i}^3$. The second chain is generated by the rigid rotation mode around beam axis, $\tilde{\boldsymbol{d}}_0^{torsion}$, with its linear part $\tilde{\boldsymbol{d}}_1^{torsion}$ representing the constant out-of-plane wrapping field typical of torsional deformation. The third and fourth chain are both composed by four eigenvectors and are originated from two transverse rigid motion modes, $\tilde{\boldsymbol{d}}_0^{bend1}$ and $\tilde{\boldsymbol{d}}_0^{bend2}$ respectively, with their linear components $\tilde{\boldsymbol{d}}_1^{bend1}$ and $\tilde{\boldsymbol{d}}_1^{bend2}$ representing the rigid rotations of the cross-section around axis $\boldsymbol{i}^1$ and $\boldsymbol{i}^2$ axis, respectively.

The solution of the equation (22) corresponding to a 4-th order Jordan block can thus be expressed as a polynomial of eigenvectors $\tilde{\boldsymbol{d}}_i$.

$$
\hat{\boldsymbol{u}} = \begin{bmatrix} \tilde{\boldsymbol{d}}_0 & \tilde{\boldsymbol{d}}_1 & \tilde{\boldsymbol{d}}_2 & \tilde{\boldsymbol{d}}_3 \end{bmatrix}
\begin{bmatrix}
1 & z & z^2/2 & z^3/3! \\
0 & 1 & z & z^2/2 \\
0 & 0 & 1 & z \\
0 & 0 & 0 & 1
\end{bmatrix}
\begin{Bmatrix}
k_0 \\ k_1 \\ k_2 \\ k_3
\end{Bmatrix},
\tag{42}
$$

where $\boldsymbol{k}_i$ is the magnitude of eigenvector $\tilde{\boldsymbol{d}}_i$. As already discussed, the terms $(\tilde{\boldsymbol{d}}_0 z + \tilde{\boldsymbol{d}}_1)k_1$ and $\tilde{\boldsymbol{d}}_0 k_0$ correspond to rigid out-of-plane rotation and rigid in-plane translation, so they are associated with null strain and stress, and have no contribution to deformation. Therefore k_0 and k_1 will not appear in the definition of the internal work and the amplitudes of the parabolic and cubic terms, k_2 and k_3, could be interpreted as generalized section deformation parameters. This is in agreement with the classical solution of beam bending problem that only the second and third derivatives of the displacement contribute to bending deformation. For the 2-nd order Jordan block, only k_1 contributes to deformation. Substituting equation (42) and its derivative with respect to z into equation (37), yields

$$\tilde{\boldsymbol{q}} = \begin{bmatrix} \tilde{\boldsymbol{\chi}}_0 & \tilde{\boldsymbol{\chi}}_1 & \tilde{\boldsymbol{\chi}}_2 & \tilde{\boldsymbol{\chi}}_3 \end{bmatrix} \begin{bmatrix} 1 & z & z^2/2 & z^3/3! \\ 0 & 1 & z & z^2/2 \\ 0 & 0 & 1 & z \\ 0 & 0 & 0 & 1 \end{bmatrix} \begin{Bmatrix} k_0 \\ k_1 \\ k_2 \\ k_3 \end{Bmatrix}, \tag{43}$$

where $\tilde{\boldsymbol{\chi}}_0 = \begin{Bmatrix} \boldsymbol{0} \\ \tilde{\boldsymbol{d}}_0 \end{Bmatrix}$ and $\tilde{\boldsymbol{\chi}}_i = \begin{Bmatrix} \tilde{\boldsymbol{d}}_{i-1} \\ \tilde{\boldsymbol{d}}_i \end{Bmatrix}$. As discussed above, among the twelve eigenvectors, only six do contribute to deformation, thus the wrapping displacement field can be expressed as

$$\tilde{\boldsymbol{q}}_d = \tilde{\boldsymbol{Q}}_d \boldsymbol{k}_d \tag{44}$$

where

$$\tilde{\boldsymbol{Q}}_d = \begin{bmatrix} \tilde{\boldsymbol{d}}_0^{axis} & \tilde{\boldsymbol{d}}_0^{torsion} & \tilde{\boldsymbol{d}}_1^{bend1} & \tilde{\boldsymbol{d}}_2^{bend1} & \tilde{\boldsymbol{d}}_1^{bend2} & \tilde{\boldsymbol{d}}_2^{bend2} \\ \tilde{\boldsymbol{d}}_1^{axis} & \tilde{\boldsymbol{d}}_1^{torsion} & \tilde{\boldsymbol{d}}_2^{bend1} & \tilde{\boldsymbol{d}}_3^{bend1} & \tilde{\boldsymbol{d}}_2^{bend2} & \tilde{\boldsymbol{d}}_3^{bend2} \end{bmatrix} \tag{45}$$

and vector $\boldsymbol{k}_d$ represents the magnitude of the six deformable eigenvectors. By appending the zero nodal values of electric potential, magnetic potential and temperature into eigenvectors $\tilde{\boldsymbol{d}}_i$ it is thus possible to build six generalized eigenvector $\boldsymbol{d}_i$, with the homogeneous solution corresponding to polynomial deformation equal to

$$\hat{\boldsymbol{q}}_d = \boldsymbol{Q}_d \boldsymbol{k}_d. \tag{46}$$

$\boldsymbol{Q}_d$ is consisted by generalized eigenvector $\boldsymbol{d}_i$, and has the same structure with $\tilde{\boldsymbol{Q}}_d$.

5.2. *Particular solutions*

Particular solutions can be obtained by applying constant electric (magnetic or temperature) potential on each independent electric (magnetic or temperature) region's electrode. The number of particular solutions is as many as the number of independent regions corresponding to electric, magnetic and temperature fields. For a multiphysics beam cross-section, for example, in order to compute the particular solution corresponding to the electric field, one should apply an unit voltage difference to the electrodes of one independent piezoelectric region, while keeping all other electrodes grounded (both the electric, magnetic and temperature fields). The temperature is assumed to be independent from the deformation, from the electric field and from the magnetic field. In other words, only one-way coupling is considered for the temperature field, and the temperature difference must be kept equal to 0 when computing the particular solutions corresponding to the electric and magnetic fields. Since the electric or magnetic potential are constant with respect to z, the corresponding solution is constant as well. Thus

$$
\boldsymbol{E} \left\{ \begin{array}{c} \hat{\boldsymbol{u}} \\ \hat{\boldsymbol{\phi}} \\ \hat{\boldsymbol{\psi}} \\ \boldsymbol{0} \end{array} \right\}_{\phi} = \left\{ \begin{array}{c} \boldsymbol{0} \\ \hat{\boldsymbol{P}}_{\phi} \\ \hat{\boldsymbol{P}}_{\psi} \\ \boldsymbol{0} \end{array} \right\} \tag{47}
$$

defines the constant solution, the subscript ϕ means that it is a particular solution corresponding to electric filed. And

$$
\hat{\boldsymbol{q}}_{\phi} = \left\{ \begin{array}{c} \boldsymbol{0}_{N \times 1} \\ \left\{ \begin{array}{c} \hat{\boldsymbol{u}} \\ \hat{\boldsymbol{\phi}} \\ \hat{\boldsymbol{\psi}} \\ \boldsymbol{0} \end{array} \right\}_{\phi} \end{array} \right\} . \tag{48}
$$

Matrix $\boldsymbol{Q}_{\phi}$ can be obtained by stacking all the $\hat{\boldsymbol{q}}_{\phi}$ column by column. The same procedure can be applied to compute $\boldsymbol{Q}_{\psi}$ and $\boldsymbol{Q}_T$.

6. Sectional characteristics

Vector $\boldsymbol{k}_d$ is not energetically conjugated to the sectional stress resultant vector $\boldsymbol{\vartheta}$. It is however possible to find a coordinate transformation matrix $\boldsymbol{G}_{\varphi}$, such that $\boldsymbol{\varphi} = \boldsymbol{G}_{\varphi}^{-1} \boldsymbol{k}_d$ is the deformation energetically conjugated to $\boldsymbol{\vartheta}$. Matrix $\boldsymbol{G}_{\varphi}$ can be determined by imposing the energy equivalence of a short-circuited beam. On one hand, the virtual internal work can be computed as

$$
\begin{aligned}
\delta L_{is} &= \int_L \delta \hat{\boldsymbol{q}}^T \boldsymbol{K}_{FEM} \hat{\boldsymbol{q}} \mathrm{d}z = \int_L \delta \hat{\boldsymbol{q}}_d^T \boldsymbol{K}_{FEM} \hat{\boldsymbol{q}}_d \mathrm{d}z \\
&= \int_L \delta \boldsymbol{k}_d^T \boldsymbol{Q}_d^T \boldsymbol{K}_{FEM} \boldsymbol{Q}_d \boldsymbol{k}_d \mathrm{d}z \\
&= \int_L \delta \boldsymbol{\varphi}^T \boldsymbol{G}_{\varphi}^T \boldsymbol{Q}_d^T \boldsymbol{K}_{FEM} \boldsymbol{Q}_d \boldsymbol{G}_{\varphi} \boldsymbol{\varphi} \mathrm{d}z
\end{aligned} \tag{49}
$$

On the other hand, the virtual internal work can be computed by the product of average sectional resultant vector $\boldsymbol{\vartheta}$ with the virtual variation of its work-conjugated deformation parameter $\boldsymbol{\varphi}$, that is

$$
\delta L_{is} = \int_L \delta \boldsymbol{\varphi}^T \boldsymbol{\vartheta} \mathrm{d}z, \tag{50}
$$

where $\boldsymbol{\theta}$ is expressed as

14

$$\begin{aligned}
\boldsymbol{\vartheta} &= \int_A \begin{bmatrix} \boldsymbol{I} \\ \boldsymbol{x} \times \end{bmatrix} \boldsymbol{S} \cdot \boldsymbol{n} \mathrm{d}A \\
&= \int_A \begin{bmatrix} \boldsymbol{I} \\ \boldsymbol{x} \times \end{bmatrix} (\boldsymbol{\Gamma} : \boldsymbol{\epsilon}) \cdot \boldsymbol{n} \mathrm{d}A \\
&= \int_A \begin{bmatrix} \boldsymbol{I} \\ \boldsymbol{x} \times \end{bmatrix} \boldsymbol{n} \cdot \boldsymbol{\Gamma} \cdot \boldsymbol{n} \cdot \boldsymbol{x}'_{,z} \mathrm{d}A \\
&\quad + \int_A \begin{bmatrix} \boldsymbol{I} \\ \boldsymbol{x} \times \end{bmatrix} \boldsymbol{n} \cdot \boldsymbol{\Gamma} \cdot \mathrm{grad}_S(\boldsymbol{x}') \mathrm{d}A \\
&= \begin{bmatrix} \boldsymbol{L}^T & \boldsymbol{R}^T \end{bmatrix} \hat{\boldsymbol{q}}_d.
\end{aligned} \tag{51}$$

where L and R are given in A. By equating equation (49) and equation (50), yields

$$\begin{aligned}
\delta\boldsymbol{\varphi}^T \boldsymbol{G}_\varphi^T \boldsymbol{Q}_d^T \boldsymbol{K}_{FEM} \boldsymbol{Q}_d \boldsymbol{G}_\varphi \boldsymbol{\varphi} &= \delta\boldsymbol{\varphi}^T \boldsymbol{\vartheta} \\
&= \delta\boldsymbol{\varphi}^T \begin{bmatrix} \boldsymbol{L}^T & \boldsymbol{R}^T \end{bmatrix} \boldsymbol{Q}_d \boldsymbol{G}_\varphi \boldsymbol{\varphi}
\end{aligned} \tag{52}$$

Equation (52) must be satisfied for any possible deformations, so it is equivalent to a system of linear equations with the columns of matrix $\boldsymbol{G}_\varphi$ as unknowns.

$$\boldsymbol{Q}_d^T \boldsymbol{K}_{FEM} \boldsymbol{Q}_d \boldsymbol{G}_\varphi = \boldsymbol{Q}_d^T \begin{Bmatrix} \boldsymbol{L} \\ \boldsymbol{R} \end{Bmatrix}. \tag{53}$$

After substituting $\boldsymbol{G}_\varphi$ into equation (31), the generalized beam stiffness matrix can be finally computed by

$$\boldsymbol{K}_{BEAM} = \boldsymbol{G}^T \boldsymbol{Q}^T \boldsymbol{K}_{FEM} \boldsymbol{Q} \boldsymbol{G} \tag{54}$$

where $\boldsymbol{Q} = \begin{bmatrix} \boldsymbol{Q}_d & \boldsymbol{Q}_\phi & \boldsymbol{Q}_\psi & \boldsymbol{Q}_T \end{bmatrix}$ and

$$\boldsymbol{G} = \begin{bmatrix} \boldsymbol{G}_\varphi & \boldsymbol{0} & \boldsymbol{0} & \boldsymbol{0} \\ \boldsymbol{0} & \boldsymbol{I} & \boldsymbol{0} & \boldsymbol{0} \\ \boldsymbol{0} & \boldsymbol{0} & \boldsymbol{I} & \boldsymbol{0} \\ \boldsymbol{0} & \boldsymbol{0} & \boldsymbol{0} & \boldsymbol{I} \end{bmatrix}. \tag{55}$$

7. Stress recovery

This section details the procedure for recovering the three dimensional stress state as a function of the imposed electric or magnetic potential, boundary temperature and cross section stress resultant and moment resultant. The sought internal force $\boldsymbol{t}$ and moment $\boldsymbol{m}$ at a given section are equal, by definition, to the stress vector resultant and moment resultant over the cross-section:

$$\int_A \begin{bmatrix} \boldsymbol{I} \\ \boldsymbol{x} \times \end{bmatrix} \boldsymbol{S} \cdot \boldsymbol{n} \mathrm{d}A = \begin{bmatrix} \boldsymbol{t} \\ \boldsymbol{m} \end{bmatrix}. \tag{56}$$

From Section 5, we know that the displacement is the sum of homogeneous solution $\hat{\boldsymbol{q}}_d$ and particular solution $\hat{\boldsymbol{q}}_p$:

$$\hat{\boldsymbol{q}} = \underbrace{\boldsymbol{Q}_d \boldsymbol{G}_\varphi \boldsymbol{\varphi}}_{\hat{\boldsymbol{q}}_d} + \underbrace{\boldsymbol{Q}_\phi \boldsymbol{\phi}_c + \boldsymbol{Q}_\psi \boldsymbol{\psi}_c + \boldsymbol{Q}_T \boldsymbol{T}_c}_{\hat{\boldsymbol{q}}_p} \tag{57}$$

Therefore, the total sectional resultant can be superimposed by the component induced by $\hat{\boldsymbol{q}}_d$ and $\hat{\boldsymbol{q}}_p$ respectively. The sectional resultant component corresponding to $\hat{\boldsymbol{q}}_d$ has been defined by equation (51). Substituting $\hat{\boldsymbol{q}}_p$ into equation (1, 3, 9), one can compute the stress tensor $\boldsymbol{S}_p$ induced by $\hat{\boldsymbol{q}}_p$. Integrating $\boldsymbol{S}_p$ over the cross-section and combining this integral with equation (51, 56) yields a set of linear equations with the generalized deformation $\boldsymbol{k}_d$ as unknowns:

$$\begin{bmatrix} \boldsymbol{L}^T & \boldsymbol{R}^T \end{bmatrix} \boldsymbol{Q}_d \boldsymbol{k}_d + \int_A \begin{bmatrix} \boldsymbol{I} \\ \boldsymbol{x} \times \end{bmatrix} \boldsymbol{S}_p \cdot \boldsymbol{n} \mathrm{d}A = \begin{bmatrix} \boldsymbol{t} \\ \boldsymbol{m} \end{bmatrix}. \tag{58}$$

Once $\boldsymbol{k}_d$ is computed from equation (58) the multiphysics fields quantities of the smart beam can be recovered by equation (57).

8. Examples

In this section, the proposed method is used to predict smart beam cross-section characteristics and corresponding multiphysics fields variables. All the simulations are leveraging the python interface of DOLFIN (Logg et al., 2012), a library developed within project FENICS (Alnæs et al., 2015). The material properties will be used in this paper are listed in Table 1, and the properties are expressed in a local material coordinate frame with the polarization direction along the local z axis (Wang and Yu, 2012; Kondaiah et al., 2012; Ke et al., 2014). The notations in Table 1 are consistent with equation (9). The computations were executed on a desktop computer Intel(R) Core(TM) i7 CPU 930 @ 2.80GHz. Table 2 compares the computation time cost of the different examples with those of the corresponding three dimensional Abaqus models.

8.1. *Example 1 : Homogeneous tube under axisymmetric temperature load*

This example is to demonstrate the validity of proposed method for the thermoelastic problems. Consider a homogeneous tube, as shown in Figure 2, subjected to a uniform temperature distribution on the internal and outer surface. The analytical solution for the temperature distribution along the radius is given in (Kreith et al., 2012), that is

$$T_r = T_i - \frac{T_i - T_e}{\ln{(r_e/r_i)}} \ln(r/r_i), \tag{59}$$

16

Table 1.: Material properties

Properties	Aluminum	Steel	PZT-4	PZT-5H	$CoFe_2O_4$	$BaTiO_3/CoFe_2O_4$ composite
$E_{11} = E_{22}$, GPa	68.9	210	81.3	62.05	154.3	135.1
E_{33}, GPa	68.9	210	64.5	57.16	142.8	130.7
$G_{13} = G_{23}$, GPa	27.56	80.15	25.6	23.0	45.3	45.0
G_{12}, GPa	27.56	80.15	30.6	23.0	56.5	50.0
ν_{12}	0.25	0.31	0.329	0.334	0.366	0.351
$\nu_{13} = \nu_{23}$	0.25	0.31	0.432	0.409	0.401	0.369
$d_{311} = d_{322}$, Cm^{-2}	0	0	-5.2	-6.5	0	-3.0
d_{333}, Cm^{-2}	0	0	15.08	23.2	0	7.0
$d_{212} = d_{123}$, Cm^{-2}	0	0	12.7	17.0	0	0
$\epsilon_{11} = \epsilon_{22}$, Fm^{-1}	0	0	6.761E-9	1.503E-8	0.08E-9	0.8E-9
ϵ_{33}, Fm^{-1}	0	0	5.874E-9	1.300E-8	0.093E-9	5.0E-9
$q_{311} = q_{322}$, $NA^{-1}m^{-1}$	0	0	0	0	580.3	300.0
q_{333}, $NA^{-1}m^{-1}$	0	0	0	0	699.7	380.0
$q_{212} = q_{123}$, $NA^{-1}m^{-1}$	0	0	0	0	550.0	220.0
$\mu_{11} = \mu_{22}$, $C^2N^{-1}m^{-2}$	0	0	5.0E-6	5.0E-6	590.0E-6	250.0E-6
μ_{33}, $C^2N^{-1}m^{-2}$	0	0	10.0E-6	10.0E-6	157.0E-6	100.0E-6
$m_{11} = m_{22}$, $CA^{-1}m^{-2}$	0	0	0	0	0	4.8E-12
m_{33}, $CA^{-1}m^{-2}$	0	0	0	0	0	2.75E-9
$\beta_{11} = \beta_{22}$, K^{-1}	2.4E-5	1.2E-5	3.589E-6	2.2E-6	10.0E-6	11.8E-6
β_{33}, K^{-1}	2.4E-5	1.2E-5	3.938E-6	2.2E-6	10.0E-6	8.6E-6
p_2, $Cm^{-2}K^{-1}$	0	0	0	0	0	-6.5E-7
k_2, $Cm^{-2}K^{-1}$	0	0	0	0	0	-28.0E-5

Table 2.: Time cost

Example NO.	Abaqus computation time	Stiffness computation time	Recovery time
1	488 s	64.0 s	14.1 s
2	523 s	7.3 s	1.2 s
3	631 s	26.9 s	5.4 s
4	700 s	34.4 s	5.6 s
5 EAM	717 s	8.8 s	1.8 s
5 SAM	815 s	8.4 s	1.7 s
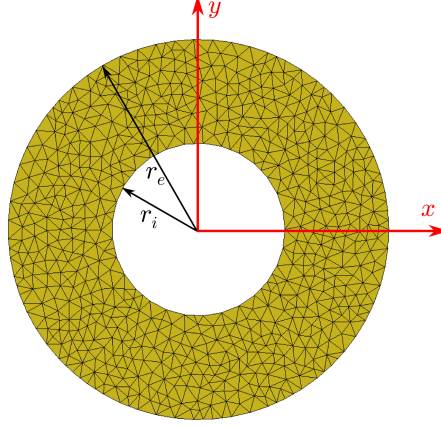
Figure 2.: Homogeneous tube cross-section mesh.
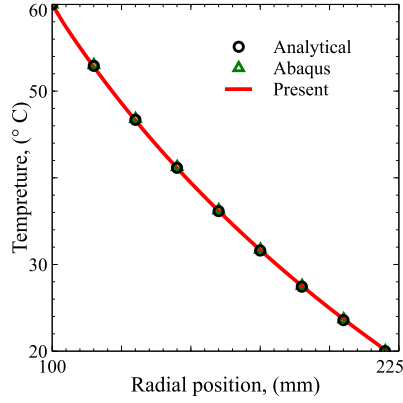
Figure 3.: Temperature distribution along the radius of homogeneous tube.

where $r_i = 100$ mm, $r_e = 220$ mm, $T_i = 60\,°\text{C}$ and $T_e = 20\,°\text{C}$ are the internal radius, the exterior radius and the corresponding prescribed temperature. The analytical solution of the thermal stress of homogeneous tube is derived in B. An additional comparison is performed with respect to a three dimensional finite element Abaqus model, with an overall beam length of 2 m and sampling the stress in the middle of the beam in order to get rid of any boundary effect, 88445 quadratic brick elements were used. Since triangular elements are used in this example a much more fined mesh 7796 elements were employed, rather than mesh depicted in Figure 2, in order to get a smooth curve along y-axis. Figure 3 and Figure 4 compare the computed temperature and stress components distributions with that from the analytical solutions and the Abaqus model, at $x = 0$ mm along the radius. The results show a considerable agreement is achieved.

8.2. *Example 2 : Bimetallic beam under thermal load*

This example refers to a rectangular cross-section beam of length 100 mm stacked by a steel layer and an aluminum alloy layer, as shown in Figure 5. Each layer is 6 mm wide and 1.5 mm thick. Two thermal load cases will be studied in this example. In the first case the beam is subjected to a uniform temperature of $100\,°\text{C}$; in the second case the beam top and bottom surface have a prescribed temperature of $100\,°\text{C}$ and $0\,°\text{C}$,

| (a) σ_{xx} | (b) σ_{yy} | (c) σ_{zz} |
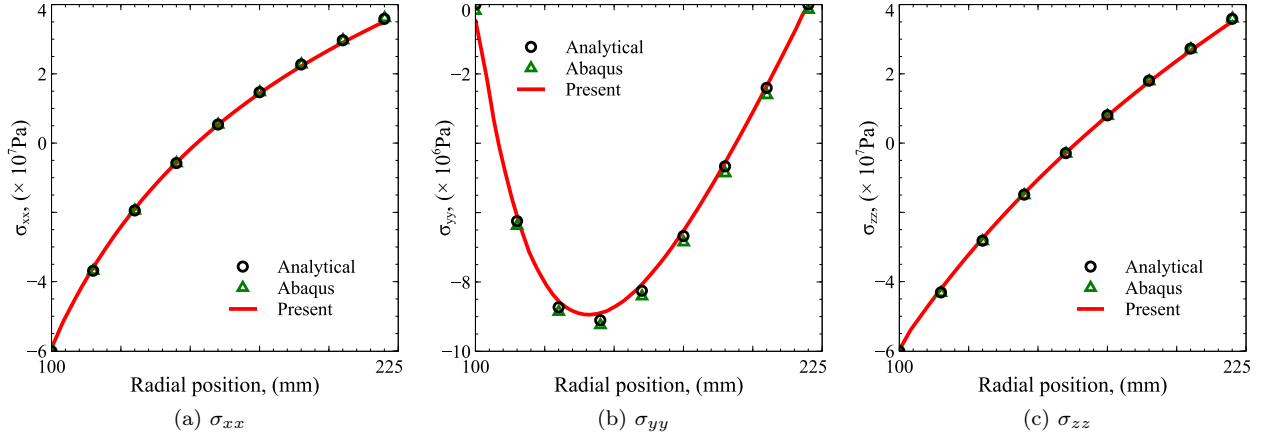
Figure 4.: Stress distribution along the radius of homogeneous tube.
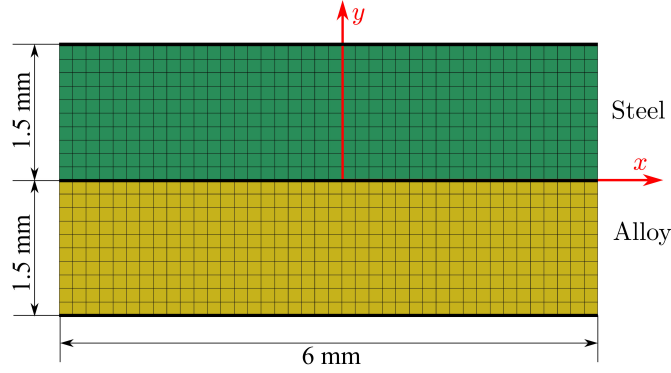
Figure 5.: Bimetallic beam section-section mesh.

respectively. A mesh with 40×20 parabolic quadrilateral elements are used. The three dimensional quantities are recovered by following the procedure outlined in Section 7. As a comparison, a thermal-displacement coupling simulation is run based on a three dimensional solid finite element model composed of 96000 quadratic brick elements using Abaqus. Figure 6 shows the through-thickness three dimensional stress components distributions along the line $x = 0$ mm at mid-span under uniform thermal load. For the second case of prescribed temperature Figure 7 and Figure 8 show the temperature and stress components distributions, respectively. Excellent agreements exist between the results obtained by the present method and Abaqus' three dimensional analysis.

8.3. *Example 3 : Two-layer piezoelectric beam*

An two-layer piezoelectric beam in (Wang and Yu, 2012) is investigated which is composited by an aluminum layer and a PZT-4 layer. The beam cross-section is square as shown in Figure 9. Each layer has a thickness of 0.05 m and a width of 0.1 m. The beam length is equal to 1.0 m. The beam axis is along the global z direction, and the polarization direction of PZT-4 is through the beam thickness. The interface between the two layers is grounded, and at the top surface of the PZT-4 patch a volt-

19
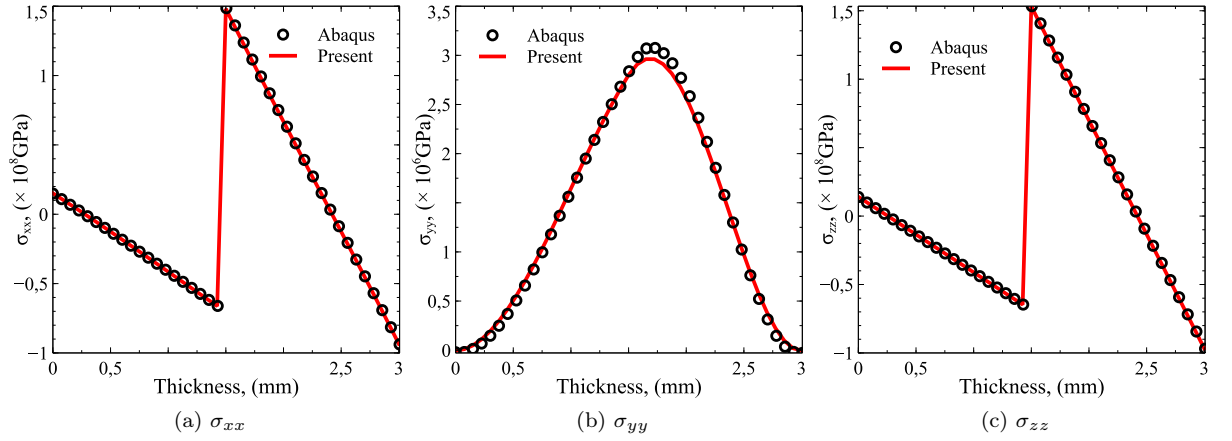
Figure 6.: Stress distributions of bimetallic beam along the thickness under uniform thermal load.
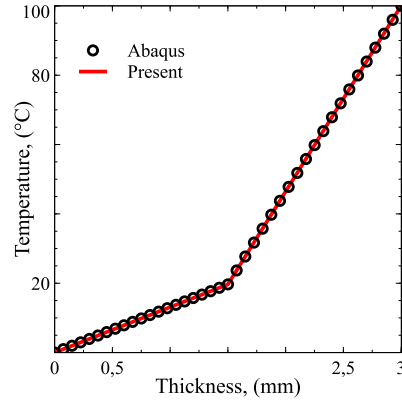
Figure 7.: Temperature distribution of bimetallic beam along the thickness under prescribed surface temperature.
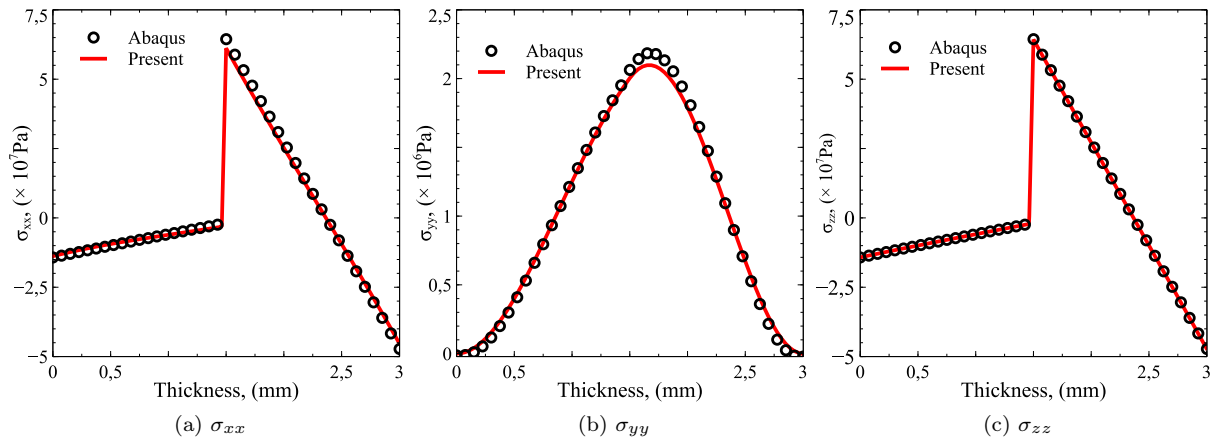
Figure 8.: Stress distributions of bimetallic beam along the thickness under prescribed surface temperature.

20
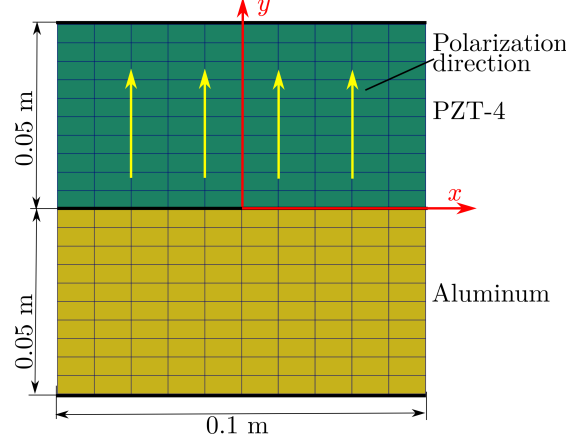
Figure 9.: Two-layer piezoelectric beam cross-section.

age of 500 V is applied. The mesh is built with 80000 C3D20E and C3D20 20-nodes quadratic piezoelectric brick elements in Abaqus, while 10×20 parabolic quadrilateral elements are used in the present method. The cross-section stiffness constants calculated by present method are listed in Table 3, where EA is the extension stiffness, GJ is the torsional stiffness, EJ_x and EJ_y are the bending stiffness, GA_x and GA_y are the shear stiffness and $K_{T_x M_z}$ and $K_{T_z M_x}$ are the shear-torsional and extensional-bending coupling stiffness, respectively. There exists significant coupling between extension and electric potential, as well as bending and electric load characterized by T_{zV} and M_{xV}, thus the beam is expected to stretch along axis z and bend when the external voltage is applied. The recovered three dimensional stress are plotted in Figure 10. The present stress results are also compared with results obtained by VABS (Cesnik and Hodges, 1997) (a cross sectional analysis tool for composite beams) from (Wang and Yu, 2012). In order to compare with VABS, we adopted the same mesh(200 parabolic quadrilateral elements) used in (Wang and Yu, 2012). It can be observed that the present method achieves an excellent coincidence both with three dimensional Abaqus analysis and VABS.

In order to demonstrate that the present method can deal with reasonably short beams, the stress distributions of the free end beam cross-section have been studied for varying beam lengths, while keeping cross-section unchanged. The three dimensional Abaqus model is clamped at one end, thus one can expect that the stress distribution at the free end will be influenced by the constraint for very short beams. The results obtained by using Abaqus and the present method are reported in Figure 11, where L is the beam length, and a is the side length of the square cross-section. It can be noticed that the results obtained with the present method match Abaqus' ones when the beam is length is at least twice the cross-section size. As already discussed in Section 5, the exponential solutions only have influence within limited domain, and then rapidly decay along the beam axis.

8.4. *Example 4 : Magneto-electro-elastic beam*

In this example, a magneto-electro-elastic beam of the same geometry with the example given in (Wang and Yu, 2012) is studied. The beam is 0.8 m long, and made with the piezoelectric material PZT-4 and the piezomagnetic material CoFe$_2$O$_4$. The beam is composed by three layers, each with a thickness of 0.03 m, a width of 0.1m,

21

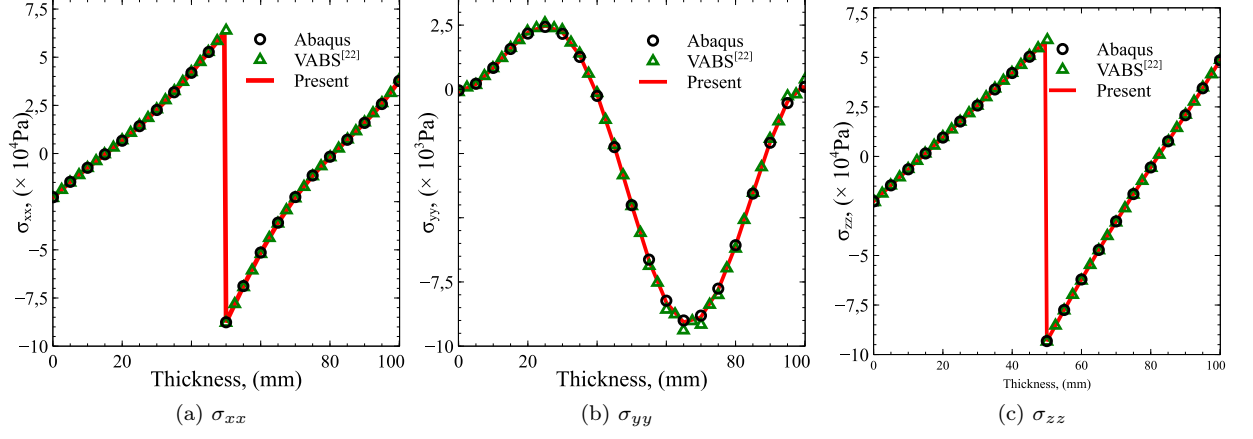(a) σ_{xx} (b) σ_{yy} (c) σ_{zz}

Figure 10.: Stress distributions of two-layer beam along the thickness.

Figure 11.: Stress distributions of two-layer beam with various length

(a) σ_{xx} (b) σ_{yy} (c) σ_{zz}
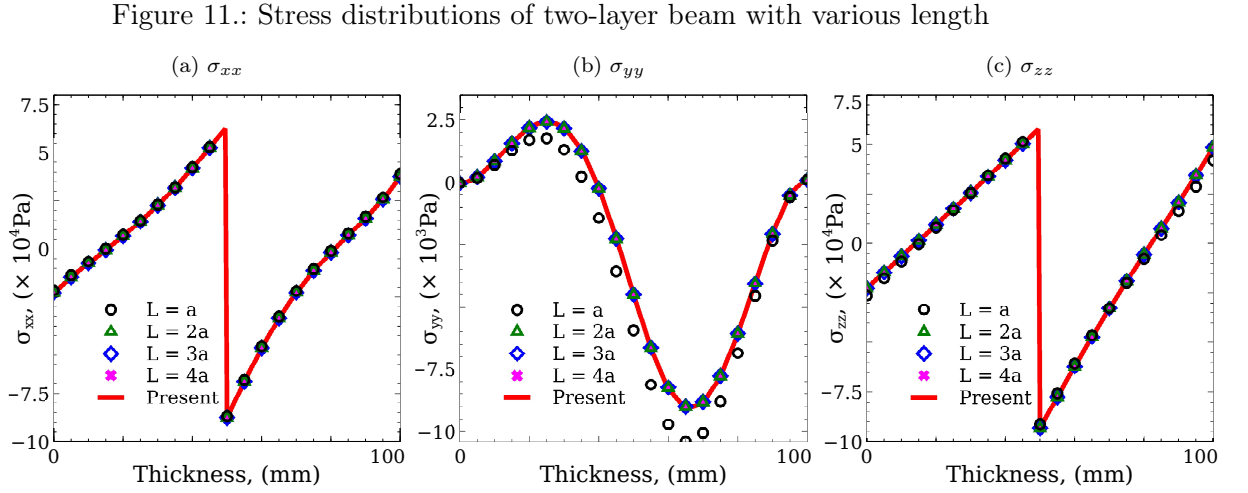
Table 3.: Cross-section stiffness of two-layer beam.

Properties	present
EA, N	7.512241E+8
GJ, Nm^2	3.901666E+5
EJ_x, Nm^2	6.374177E+5
EJ_y, Nm^2	6.259304E+5
GA_x, N	2.402594E+8
GA_y, N	2.293800E+8
$K_{T_x M_z}$, Nm	-3.286010E+5
$K_{T_z M_x}$, Nm	1.538324E+6
T_{zV}, Cm	-1.009702
M_{xV}, C	-2.447229E-2
C_{vv}, Fm^{-1}	2.0179360E-8

and with a stacking sequence of PZT-4/CoFe$_2$O$_4$/PZT-4. In order to maintain symmetric, the top layer is flipped by 180°, as shown in Figure 12. The interfaces between CoFe$_2$O$_4$ and PZT-4 are grounded, and a voltage of 500V is applied to both of the top and bottom surfaces; the magnetic potential on the interfaces is assumed to be null. Both of the PZT-4 and CoFe$_2$O$_4$ layers are polarized along the beam thickness. 72000 quadratic brick elements were used in Abaqus, while 50×45 parabolic quadrilateral elements were used in the present method. Figure 13 shows the distributions of electric potential and magnetic potential over the thickness along $x = 0$ mm. Figure 14 plots the three dimensional stress distributions. Since Abaqus could not deal with piezomagnetic materials, in this example, and only for the Abaqus three dimensional solution, the piezomagnetic material was treated as an analogy of piezoelectric; this does not make the Abaqus result void because the three regions are separated by grounded electrodes. The electric potential within PZT-4 layers is distributed linearly as expected, since an almost uniform electric filed is generated between two parallel equipotential plates, while the magnetic potential induced within CoFe$_2$O$_4$ layer is antisymmetric; this result does not match that of (Wang and Yu, 2012), where the predicted magnetic potential distribution within the middle layer is symmetric. This is likely because the reference did not detail the polarization directions of each layer. However, even by permuting the three polarization direction, the result in (Wang and Yu, 2012) does not agree with that obtained by applying the present method or by using Abaqus, although the magnetic potential becomes symmetric. Note also that the stress distributions are not exactly symmetric about the x-axis, since the structure is not strictly symmetric due to the polarization directions, as shown in Figure 12.

If an additional small uniform temperature load of 1 °C is imposed to this beam, the thermal load has significant effects to the electric, magnetic potential and stress distributions, as shown in Figure 13 and Figure 14. It can be inferred that, in order to compensate for thermal deformations a considerable high voltage may be required.

As a last example, the middle CoFe$_2$O$_4$ layer is replaced by a BaTiO$_3$ − CoFe$_2$O$_4$ composite layer of the same size. The BaTiO$_3$ − CoFe$_2$O$_4$ composite do have both piezoelectric and piezomagnetic characteristics. When the same electric potential is applied, the electric potential, magnetic potential and stress distributions are shown in Figure 15 and Figure 16; only the result obtained by the present method are reported since there are no available results to compare. The middle layer shows both electric and magnetic induced fields.
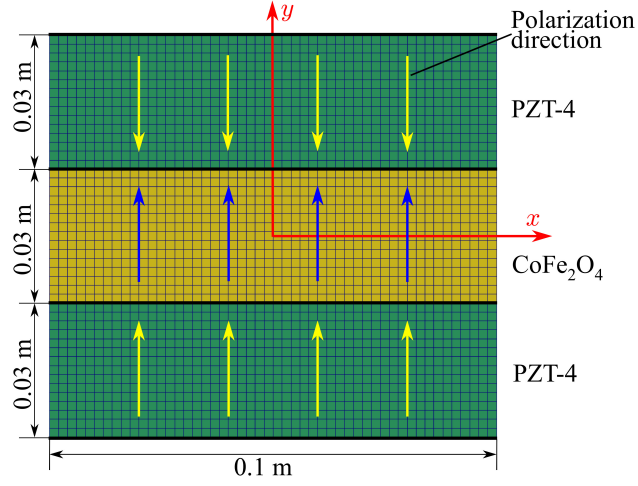
23

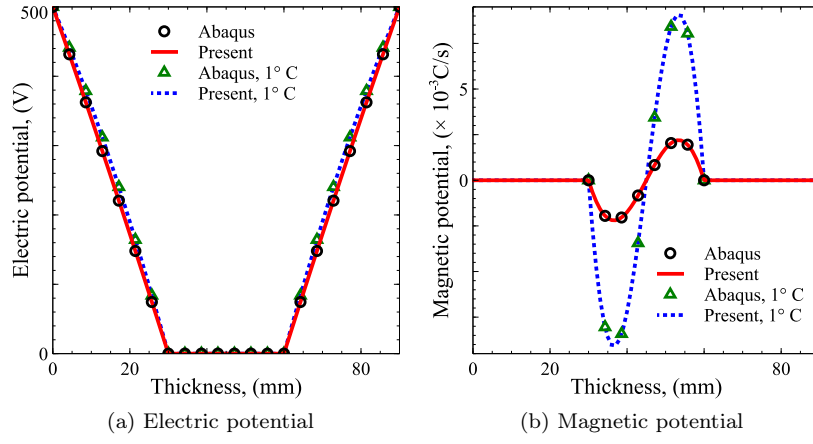Figure 12.: magneto-electro-elastic beam cross-section.

(a) Electric potential

(b) Magnetic potential

Figure 13.: Electric potential and magnetic potential distributions of magneto-electro-elastic beam along the thickness(PZT-4/CoFe$_2$O$_4$/PZT-4).
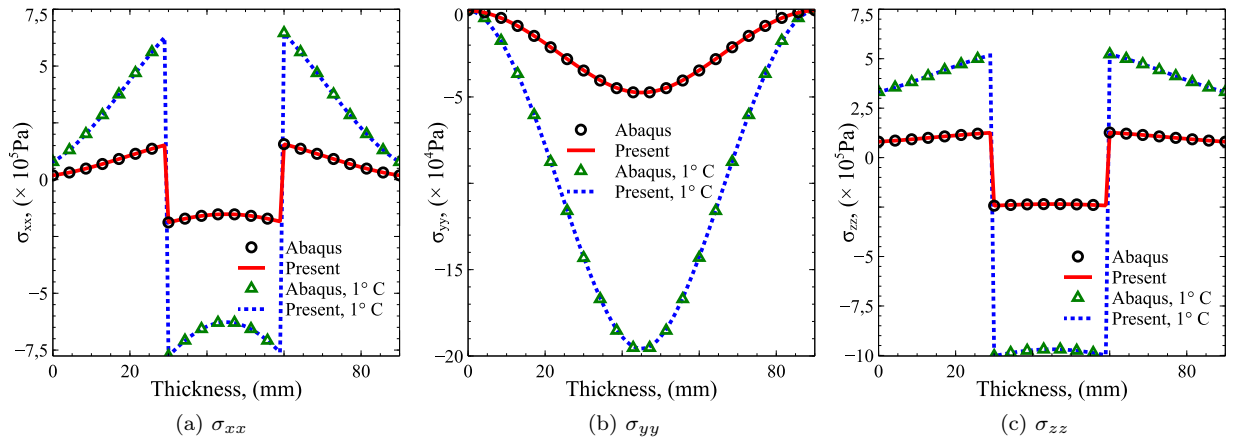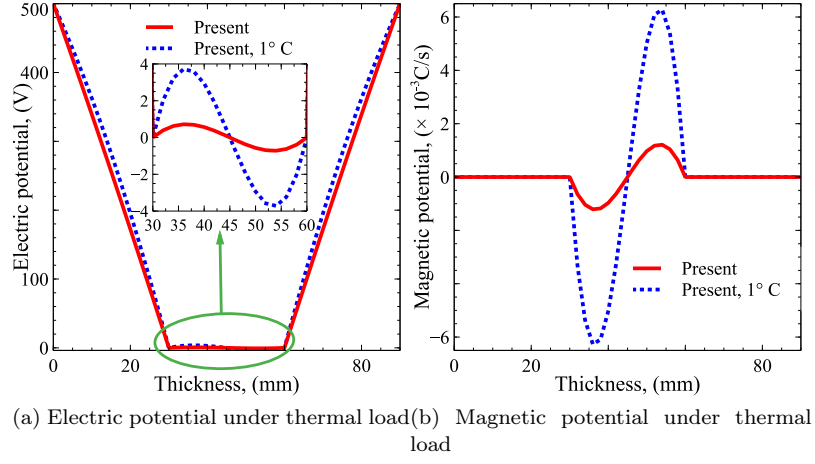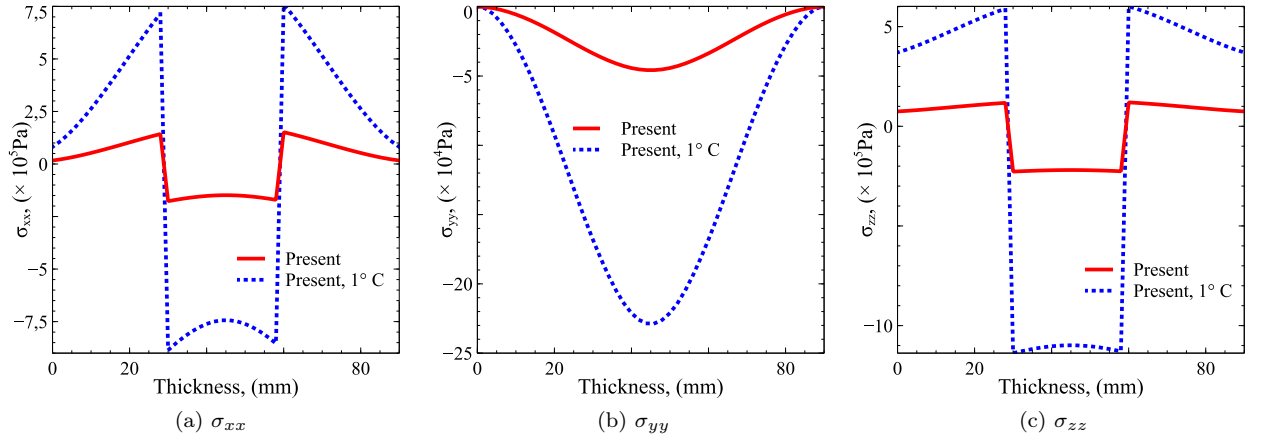

(a) σ_{xx}

(b) σ_{yy}

(c) σ_{zz}

Figure 14.: Stress distributions of magneto-electro-elastic beam along the thickness(PZT-4/CoFe$_2$O$_4$/PZT-4).

(a) Electric potential under thermal load(b) Magnetic potential under thermal
load

Figure 15.: Electric potential and magnetic potential distributions of magneto-electro-elastic beam along the thickness(PZT-4/BaTiO$_3$ − CoFe$_2$O$_4$/PZT-4).

(a) σ_{xx} (b) σ_{yy} (c) σ_{zz}

Figure 16.: Stress distributions of magneto-electro-elastic beam along the thickness(PZT-4/BaTiO$_3$ − CoFe$_2$O$_4$/PZT-4).

25

Figure 17.: Beam cross-section

(a) EAM   (b) SAM
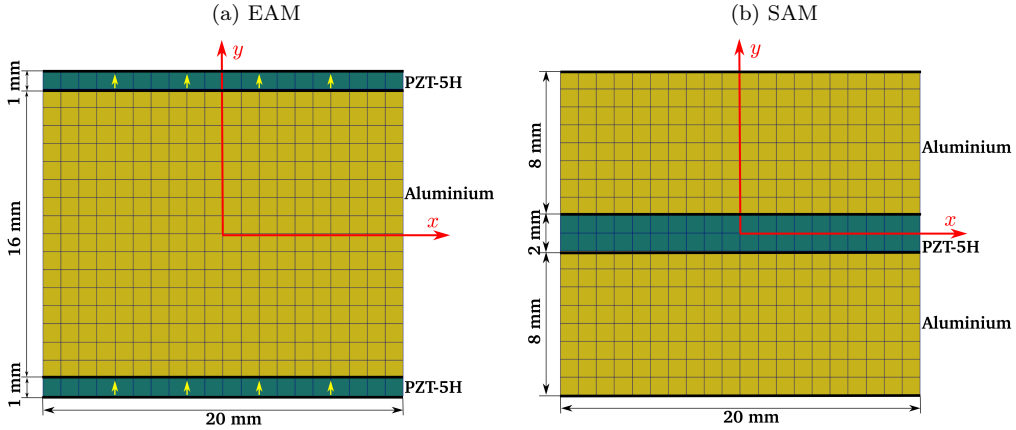
8.5. *Example 5 : EAM(Extension Actuation Mechanism) and SAM(Shear Actuation Mechanism) piezoelectric beam*

In this example, two types of piezoelectric actuators are considered which are EAM and SAM. EAM uses d_{31} or d_{33} effect (here we restrict our discussion to d_{31} type piezoelectric materials), is usually surface-mounted and is known to generate longitudinal strains and thus induce extension or transverse bending; However, SAM which uses d_{51} effect, is usually of sandwich structure and generates transverse shear strains providing that the polling direction of piezoelectric components and electric field direction are perpendicular. The EAM beam is consisted by three layer with PZT-5H patches on the top and bottom, bracketing aluminum core inside; while for the SAM beam, the top and bottom are made of aluminum and a PZT-5H layer in the middle, as shown in Figure 17. Both have a width of 0.02 m and length of 0.1 m. The EAM beam is poled along thickness (y direction), and along beam axis (z direction) for SAM beam. To actuate the EAM beam, a voltage difference of $\phi_{top} - \phi_{bottom} = -10$ V is applied between top surface and bottom surface on the upper patch, and a difference of 10 V on lower patch respectively. As for the SAM a voltage difference of 20 V is applied. 80000 quadratic brick elements were used in Abaqus, while 20×18 parabolic quadrilateral elements were used in the present method. The beam spanwise displacements can be recovered by combining the current method with a Timoshenko beam model. Figure 18 compares the transverse displacements along the beam axis which obtained from present method with published works (Benjeddou et al., 1997; Kpeky et al., 2018; Carrera et al., 2018). It can be noticed that the present method achieves an excellent coincidence both with three dimensional Abaqus analysis and other methods. The SAM case, however, deserves a discussion on its own. The particular solution, shown in Figure 19 is constant along the beam axis and completely stress-free. As such, it is not a surprise that the transverse displacement of Figure 18(b) is linear, since the beam is simply rotated with respect to its constraint. This is because the particular solution cross-section displacement is characterized by a non-null average rotation of the cross section. Once this rotation is accounted for in the beam model boundary condition the solution matches that of the three dimensional analysis everywhere but near the clamped end, where the beam model cannot clearly account for the local stress distribution introduced by the constraint.

26

Figure 18.: Transverse displacement along beam axis
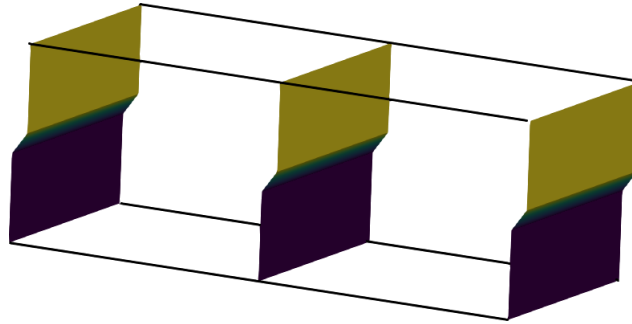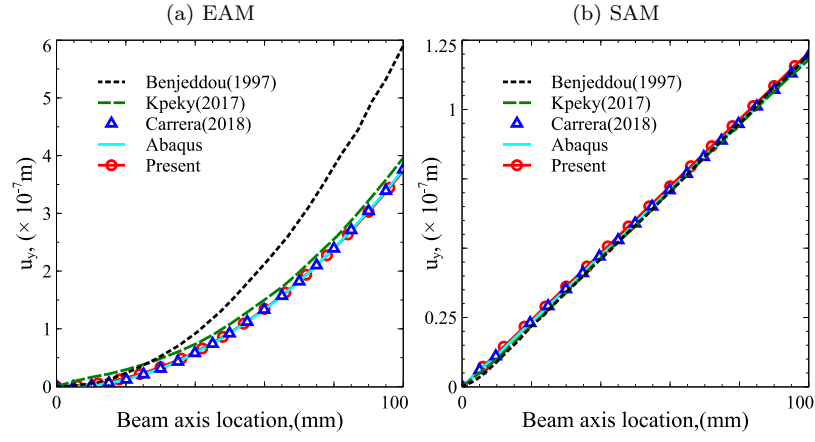
(a) EAM

(b) SAM

Figure 19.: SAM case particular solution: stress-free shear deformation constant along the beam axis.

27

9. Conclusion

This paper extended the method in (Morandini et al., 2010) to multiphysics smart beam, a fully coupled magneto-electro-elastic, as well as one-way coupling with temperature field, modeling procedure of prismatic smart beam is proposed. Originating from virtual works principle on multiphysics fields without any a-priori assumptions, this procedure leads to a set of non-homogeneous differential equations, whose solution can be decomposed to a homogeneous solution and a set of particular solutions. The homogeneous contribution can be resorted to the computation of eigenvectors corresponding to null eigenvalue, and the particular solutions can be obtained by applying unit input to each independent region. The proposed approach was validated by numerical examples by studying the distributions of multiphysics fields. The results show a good agreement with those obtained by Abaqus three dimensional finite element analysis. The proposed method can predict beam behaviors under multiphysics fields which feature significant mutual couplings. Due to its flexibility and efficiency compared with three dimensional finite element analysis, and its considerable fidelity compared with simplified formulas, the procedure proposed can be used for the stiffness computation, stress recovery, design, control and optimization of smart beams.

Acknowledgment

Appendix A. Assembled matrices

The assembled matrices used in equation (21) can be expressed as:

$$\boldsymbol{M}_{uu}(i,j) = \int_A N_{i(u)} N_{j(u)} \boldsymbol{n} \cdot \boldsymbol{\Gamma} \cdot \boldsymbol{n} \mathrm{d}A$$
$$\boldsymbol{M}_{u\phi}(i,j) = \int_A N_{i(u)} N_{j(\phi)} \boldsymbol{n} \cdot \boldsymbol{d}^{T231} \cdot \boldsymbol{n} \mathrm{d}A$$
$$\boldsymbol{M}_{u\psi}(i,j) = \int_A N_{i(u)} N_{j(\psi)} \boldsymbol{n} \cdot \boldsymbol{q}^{T231} \cdot \boldsymbol{n} \mathrm{d}A$$
$$\boldsymbol{M}_{\phi\phi}(i,j) = \int_A N_{i(\phi)} N_{j(\phi)} \boldsymbol{n} \cdot \boldsymbol{\varepsilon} \cdot \boldsymbol{n} \mathrm{d}A$$
$$\boldsymbol{M}_{\phi\psi}(i,j) = \int_A N_{i(\phi)} N_{j(\psi)} \boldsymbol{n} \cdot \boldsymbol{m} \cdot \boldsymbol{n} \mathrm{d}A$$
$$\boldsymbol{M}_{\psi\psi}(i,j) = \int_A N_{i(\psi)} N_{j(\psi)} \boldsymbol{n} \cdot \boldsymbol{\mu} \cdot \boldsymbol{n} \mathrm{d}A$$
$$\boldsymbol{M}_{TT}(i,j) = \int_A N_{i(T)} N_{j(T)} \boldsymbol{n} \cdot \boldsymbol{K} \cdot \boldsymbol{n} \mathrm{d}A$$
$$\boldsymbol{C}_{uu}(i,j) = \int_A \mathrm{grad}_S(N_{i(u)}) \cdot \boldsymbol{\Gamma} \cdot \boldsymbol{n} N_{j(u)} \mathrm{d}A$$
$$\boldsymbol{C}_{u\phi}(i,j) = \int_A \mathrm{grad}_S(N_{i(u)}) \cdot \boldsymbol{d}^{T231} \cdot \boldsymbol{n} N_{j(\phi)} \mathrm{d}A$$
$$\boldsymbol{C}_{u\psi}(i,j) = \int_A \mathrm{grad}_S(N_{i(u)}) \cdot \boldsymbol{q}^{T231} \cdot \boldsymbol{n} N_{j(\psi)} \mathrm{d}A$$
$$\boldsymbol{C}_{uT}(i,j) = \int_A N_{i(u)} \boldsymbol{n} \cdot (\boldsymbol{\Gamma} : \boldsymbol{\alpha}) N_{j(T)} \mathrm{d}A$$
$$\boldsymbol{C}_{\phi u}(i,j) = \int_A \mathrm{grad}_S(N_{i(\phi)}) \cdot d \cdot \boldsymbol{n} N_{j(u)} \mathrm{d}A$$
$$\boldsymbol{C}_{\phi\phi}(i,j) = \int_A \mathrm{grad}_S(N_{i(\phi)}) \cdot \boldsymbol{\varepsilon} \cdot \boldsymbol{n} N_{j(\phi)} \mathrm{d}A$$
$$\boldsymbol{C}_{\phi\psi}(i,j) = \int_A \mathrm{grad}_S(N_{i(\phi)}) \cdot \boldsymbol{m} \cdot \boldsymbol{n} N_{j(\psi)} \mathrm{d}A$$
$$\boldsymbol{C}_{\phi T}(i,j) = \int_A N_{i(\phi)} \boldsymbol{n} \cdot \boldsymbol{p} N_{j(T)} \mathrm{d}A$$
$$\boldsymbol{C}_{\psi u}(i,j) = \int_A \mathrm{grad}_S(N_{i(\psi)}) \cdot d \cdot \boldsymbol{n} N_{j(u)} \mathrm{d}A$$
$$\boldsymbol{C}_{\psi\phi}(i,j) = \int_A \mathrm{grad}_S(N_{i(\psi)}) \cdot \boldsymbol{\varepsilon} \cdot \boldsymbol{n} N_{j(\phi)} \mathrm{d}A$$
$$\boldsymbol{C}_{\psi\psi}(i,j) = \int_A \mathrm{grad}_S(N_{i(\psi)}) \cdot \boldsymbol{\mu} \cdot \boldsymbol{n} N_{j(\psi)} \mathrm{d}A$$
$$\boldsymbol{C}_{\psi T}(i,j) = \int_A N_{i(\psi)} \boldsymbol{n} \cdot \boldsymbol{k} N_{j(T)} \mathrm{d}A$$

$$\boldsymbol{C}_{TT}(i,j) = \int_A \mathrm{grad}_S(N_{i(T)}) \cdot \boldsymbol{K} \cdot \boldsymbol{n} N_{j(T)} \mathrm{d}A$$

$$\boldsymbol{C}_{Tu}^T(i,j) = \int_A N_{i(u)} \boldsymbol{n} \cdot (\boldsymbol{\Gamma} \cdot \boldsymbol{\alpha}) \cdot N_{j(T)} \mathrm{d}A$$

$$\boldsymbol{C}_{T\phi}^T(i,j) = \int_A N_{i(\phi)} \boldsymbol{n} \cdot \boldsymbol{p} N_{j(T)} \mathrm{d}A$$

$$\boldsymbol{C}_{T\psi}^T(i,j) = \int_A N_{i(\psi)} \boldsymbol{n} \cdot \boldsymbol{k} N_{j(T)} \mathrm{d}A$$

$$\boldsymbol{E}_{uu}(i,j) = \int_A \mathrm{grad}_S(N_{i(u)}) \cdot \boldsymbol{\Gamma} \cdot \mathrm{grad}_S(N_{j(u)}) \mathrm{d}A$$

$$\boldsymbol{E}_{u\phi}(i,j) = \int_A \mathrm{grad}_S(N_{i(u)}) \cdot \boldsymbol{d}^{T231} \cdot \mathrm{grad}_S(N_{j(\phi)}) \mathrm{d}A$$

$$\boldsymbol{E}_{u\psi}(i,j) = \int_A \mathrm{grad}_S(N_{i(u)}) \cdot \boldsymbol{q}^{T231} \cdot \mathrm{grad}_S(N_{j(\psi)}) \mathrm{d}A$$

$$\boldsymbol{E}_{uT}(i,j) = \int_A \mathrm{grad}_S(N_{i(u)}) \cdot (\boldsymbol{\Gamma}:\boldsymbol{\alpha}) N_{j(T)} \mathrm{d}A$$

$$\boldsymbol{E}_{\phi\phi}(i,j) = \int_A \mathrm{grad}_S(N_{i(\phi)}) \cdot \boldsymbol{\varepsilon} \cdot \mathrm{grad}_S(N_{j(\phi)}) \mathrm{d}A$$

$$\boldsymbol{E}_{\phi\psi}(i,j) = \int_A \mathrm{grad}_S(N_{i(\phi)}) \cdot \boldsymbol{m} \cdot \mathrm{grad}_S(N_{j(\psi)}) \mathrm{d}A$$

$$\boldsymbol{E}_{\phi T}(i,j) = \int_A \mathrm{grad}_S(N_{i(\phi)}) \cdot \boldsymbol{p} N_{j(T)} \mathrm{d}A$$

$$\boldsymbol{E}_{\psi\psi}(i,j) = \int_A \mathrm{grad}_S(N_{i(\psi)}) \cdot \boldsymbol{\mu} \cdot \mathrm{grad}_S(N_{j(\psi)}) \mathrm{d}A$$

$$\boldsymbol{E}_{\psi T}(i,j) = \int_A \mathrm{grad}_S(N_{i(\phi)}) \cdot \boldsymbol{k} N_{j(T)} \mathrm{d}A$$

$$\boldsymbol{E}_{TT}(i,j) = \int_A \mathrm{grad}_S(N_{i(T)}) \cdot \boldsymbol{K} \cdot \mathrm{grad}_S(N_{j(T)}) \mathrm{d}A$$

$$\boldsymbol{L}(i,j) = \int_A N_{i(u)} \boldsymbol{n} \cdot \boldsymbol{\Gamma} \cdot \boldsymbol{n} \begin{bmatrix} \boldsymbol{I} & -N_{j(u)} \boldsymbol{x}_j \times \end{bmatrix} \mathrm{d}A$$

$$\boldsymbol{R}(i,j) = \int_A \mathrm{grad}_S(N_{i(u)}) \cdot \boldsymbol{\Gamma} \cdot \boldsymbol{n} \begin{bmatrix} \boldsymbol{I} & -N_{j(u)} \boldsymbol{x}_j \times \end{bmatrix} \mathrm{d}A$$

Appendix B. Analytical solution of the thermal stresses of homogeneous tube

We report here for completeness the three dimensional stress solution for the example of Section 8.1. A more general treatment can be found in e.g. (Noda et al., 2003). Consider a three dimensional axisymmetric tube in a cylindrical coordinate system (r, θ, z). The displacement field can be expressed as

$$
\begin{aligned}
u_r(r,z) &= u(r) \\
u_\theta(r,z) &= 0 \\
u_z(r,z) &= w_1(r) + w_2(r)z
\end{aligned}
\tag{B1}
$$

The equilibrium equations are (Eslami et al., 2013)

$$
\begin{aligned}
\sigma_{r,r} + \frac{1}{r}(\sigma_r - \sigma_\theta) + \tau_{zr,z} &= 0 \\
\tau_{zr,r} + \sigma_{z,z} + \frac{\tau_{zr}}{r} &= 0
\end{aligned}
\tag{B2}
$$

For a homogeneous isotropic tube, the constitutive equation can be expressed as

$$
\begin{Bmatrix} \sigma_r \\ \sigma_\theta \\ \sigma_z \\ \tau_{zr} \end{Bmatrix} = \frac{E}{(1+\nu)(1-2\nu)} \begin{bmatrix} 1-\nu & \nu & \nu & 0 \\ \nu & 1-\nu & \nu & 0 \\ \nu & \nu & 1-\nu & 0 \\ 0 & 0 & 0 & \frac{1-2\nu}{2} \end{bmatrix} \begin{Bmatrix} \varepsilon_r - \alpha T \\ \varepsilon_\theta - \alpha T \\ \varepsilon_z - \alpha T \\ \gamma_{zr} \end{Bmatrix}
\tag{B3}
$$

The strain-displacement relationship is

$$\varepsilon_r = u_{,r}; \qquad \varepsilon_\theta = \frac{u_r}{r} + \frac{1}{r}\frac{\partial u_\theta}{\partial \theta} = \frac{u}{r}$$

$$\varepsilon_z = u_{z,z} = w_2; \qquad \gamma_{rz} = \frac{\partial u_r}{\partial z} + \frac{\partial u_z}{\partial r} = w_{1,r} + w_{2,r}z \qquad \text{(B4)}$$

Substituting equation (B4) into equation (B3), yields

$$
\begin{aligned}
\sigma_r &= au_{,r} + b(\frac{u}{r} + w_2) - (a + 2b)\alpha T \\
\sigma_\theta &= a\frac{u}{r} + b(u_{,r} + w_2) - (a + 2b)\alpha T \\
\sigma_z &= aw_2 + b(u_{,r} + \frac{u}{r}) - (a + 2b)\alpha T \\
\tau_{zr} &= G(w_{1,r} + w_{2,r}z)
\end{aligned}
\qquad \text{(B5)}
$$

where $a = \frac{E(1-\nu)}{(1+\nu)(1-2\nu)}$, $b = \frac{E\nu}{(1+\nu)(1-2\nu)}$, $G = \frac{E}{2(1+\nu)}$. The partial derivatives of the stress components are as follows

$$
\begin{aligned}
\sigma_{r,r} &= au_{,rr} + b(\frac{u_{,r}}{r} + w_{2,r}) - b\frac{u}{r^2} - (a + 2b)\alpha T_{,r} \\
\sigma_{z,z} &= 0 \\
\tau_{zr,r} &= G(w_{1,rr} + w_{2,rr}z) \\
\tau_{zr,z} &= Gw_{2,r}
\end{aligned}
\qquad \text{(B6)}
$$

Substituting equation (B5, B6) into equation (B2) leads to

$$
\begin{aligned}
a(u_{,rr} + \frac{1}{r}u_{,r} - \frac{1}{r^2}u) - (a + 2b)\alpha T_{,r} - (G + b)w_{2,r} &= 0 \qquad \text{(B7)} \\
G(w_{1,rr} + w_{2,rr}z) + \frac{G}{r}(w_{1,r} + w_{2,r}z) &= 0
\end{aligned}
$$

Therefore, one obtains

$$
\begin{aligned}
w_{1,rr} + \frac{1}{r}w_{1,r} &= 0 \\
w_{2,rr} + \frac{1}{r}w_{2,r} &= 0
\end{aligned}
\qquad \text{(B8)}
$$

Functions w_1 and w_2 can be integrated from equation (B8), that is

$$
\begin{aligned}
w_1 &= m_2 \ln(r) + m_1 \qquad \text{(B9)} \\
w_2 &= m_4 \ln(r) + m_3
\end{aligned}
$$

The shear stress τ_{zr} is zero at $r = r_i$ and $r = r_e$, which yields $m_2 = m_4 = 0$, thus w_1 and w_2 are constants. The constant w_1 do correspond to a rigid body motion, thus can

be assumed equal to zero. After re-arranging equation (B7) as

$$\frac{d}{dr}\left(\frac{1}{r}\left(\frac{d(ur)}{dr}\right)\right) = \frac{a+2b}{a}\alpha T_{,r} - \frac{G+b}{a}w_{2,r} \tag{B10}$$

the displacement u can be integrated as

$$u = c_1 r + \frac{c_2}{r} + \frac{a+2b}{a}\alpha\frac{1}{r}\int Tr\mathrm{d}r - \frac{G+b}{a}\frac{1}{r}\int w_2 r\mathrm{d}r \tag{B11}$$

Substituting equation (B11) into equation (B4), yields

$$
\begin{aligned}
\varepsilon_r &= u_{,r} = c_1 - \frac{c_2}{r^2} - \frac{a+2b}{a}\alpha\frac{1}{r^2}\int Tr\mathrm{d}r + \frac{a+2b}{a}\alpha T + \frac{G+b}{a}\frac{1}{r^2}\int w_2 r\mathrm{d}r - \frac{G+b}{a}w_2 \\
\varepsilon_\theta &= \frac{u}{r} = c_1 + \frac{c_2}{r^2} + \frac{a+2b}{a}\alpha\frac{1}{r^2}\int Tr\mathrm{d}r - \frac{G+b}{a}\frac{1}{r^2}\int w_2 r\mathrm{d}r \\
\varepsilon_z &= w_2 \\
\gamma_{rz} &= w_{1,r} + w_{2,r}z = 0
\end{aligned}
\tag{B12}
$$

Substituting equation (B12) into equation (B3), leads to

$$
\begin{aligned}
\sigma_r &= a\varepsilon_r + b(\varepsilon_\theta + \varepsilon_z) - (a+2b)\alpha T \\
&= (a+b)c_1 + \frac{b-a}{r^2}c_2 + \frac{(b-a)(a+2b)}{ar^2}\alpha\int Tr\mathrm{d}r \\
&\quad + \frac{(a-b)(G+b)}{ar^2}\int w_2 r\mathrm{d}r - Gw_2
\end{aligned}
\tag{B13}
$$

$$
\begin{aligned}
\sigma_z &= a\varepsilon_z + b(\varepsilon_r + \varepsilon_\theta) - (a+2b)\alpha T \\
&= 2bc_1 + \frac{(b-a)(a+2b)}{a}\alpha T + (a - \frac{b(G+b)}{a})w_2
\end{aligned}
\tag{B14}
$$

Substituting the expressions of a, b and G into equation (B13, B14):

$$
\begin{aligned}
\sigma_r &= \frac{E}{(1+\nu)(1-2\nu)}c_1 - \frac{E}{1+\nu}\cdot\frac{1}{r^2}c_2 - \frac{E}{(1-\nu)}\cdot\frac{1}{r^2}\alpha\int_{r_i}^r Tr\mathrm{d}r \\
&\quad + \frac{E}{2(1-\nu)(1+\nu)}\frac{1}{r^2}\int_{r_i}^r w_2 r\mathrm{d}r - \frac{E}{2(1+\nu)}w_2 \\
\sigma_\theta &= \frac{E}{(1+\nu)(1-2\nu)}c_1 - \frac{E}{1+\nu}\cdot\frac{1}{r^2}c_2 - \frac{E}{(1-\nu)}\cdot\frac{1}{r^2}\alpha\int_{r_i}^r Tr\mathrm{d}r \\
&\quad + \frac{E}{2(1-\nu)(1+\nu)}\frac{1}{r^2}\int_{r_i}^r w_2 r\mathrm{d}r - \frac{E}{2(1+\nu)}w_2 \\
\sigma_z &= \frac{2\nu E}{(1+\nu)(1-2\nu)}c_1 - \frac{E}{(1-\nu)}\alpha T + \frac{2(1-\nu)^2 E - \nu E}{2(1+\nu)(1-2\nu)(1-\nu)}w_2
\end{aligned}
\tag{B15}
$$

31

The 3 undetermined coefficients c_1, c_2, and w_2 can be computed by accounting for the natural conditions

$$
\begin{aligned}
\sigma_r|_{r=r_1} &= 0 \\
\sigma_r|_{r=r_2} &= 0 \\
\int_0^{2\pi} \int_{r_i}^{r_e} \sigma_r r \mathrm{d}r \mathrm{d}\theta &= 0
\end{aligned}
\tag{B16}
$$

Substituting equation (B15) into equation (B16), yields following set of linear equations

$$
\begin{aligned}
c_1 - \frac{1-2\nu}{r_i^2}c_2 - \frac{1-2\nu}{2}w_2 &= 0 \\
(1-\nu)c_1 - (1-\nu)(1-2\nu)\cdot\frac{1}{r_e^2}c_2 & \\
+(\frac{1-2\nu}{2}\cdot\frac{r_e^2-r_i^2}{2r_e^2} - \frac{(1-2\nu)(1-\nu)}{2})w_2 &= (1+\nu)(1-2\nu)\cdot\frac{1}{r_e^2}\alpha\int_{r_i}^{r_e} Tr\mathrm{d}r \\
\nu(1-\nu)c_1 + \frac{2(1-\nu)^2-\nu}{4}w_2 &= \frac{(1+\nu)(1-2\nu)}{r_e^2-r_i^2}\alpha\int_{r_i}^{r_e} Tr\mathrm{d}r
\end{aligned}
\tag{B17}
$$

The solution of equation (B17) is as follows

$$
\begin{aligned}
c_1 &= \frac{3(1-2\nu)}{2(1-\nu)(r_e^2-r_i^2)}\alpha\int_{r_i}^{r_e} Tr\mathrm{d}r \\
c_2 &= \frac{(1+2\nu)r_i^2}{2(1-\nu)(r_e^2-r_i^2)}\alpha\int_{r_i}^{r_e} Tr\mathrm{d}r \\
w_2 &= \frac{2}{r_e^2-r_i^2}\alpha\int_{r_i}^{r_e} Tr\mathrm{d}r
\end{aligned}
\tag{B18}
$$

where T is given by equation (59), and $\int Tr\mathrm{d}r$ can be integrated analytically

$$
\begin{aligned}
\int Tr\mathrm{d}r &= \int(T_i - \frac{T_i-T_e}{\ln(r_e/r_i)}\ln(r/r_i))r\mathrm{d}r \\
&= \frac{T_i}{2}r^2 - \frac{T_i-T_e}{\ln(r_e/r_i)}(\frac{r^2}{2}\ln(\frac{r}{r_i}) - \frac{r^2}{4})
\end{aligned}
\tag{B19}
$$

The stress components are readily computed by substituting the expressions of c_1, c_2 and w_2 into equation (B15).

References

Aldraihem, O. J. and A. A. Khdeir (2000). Smart beams with extension and thickness-shear piezoelectric actuators. *Smart Materials and Structures* 9(1), 1.

Allik, H. and T. J. Hughes (1970). Finite element method for piezoelectric vibration. *International journal for numerical methods in engineering 2*(2), 151–157.

Alnæs, M. S., J. Blechta, J. Hake, A. Johansson, B. Kehlet, A. Logg, C. Richardson, J. Ring, M. E. Rognes, and G. N. Wells (2015). The fenics project version 1.5. *Archive of Numerical Software 3*(100).

Bauchau, O. A. and J. I. Craig (2009). *Structural analysis: with applications to aerospace structures*, Volume 163. Springer Science & Business Media.

Bauchau, O. A. and S. Han (2014). Three-dimensional beam theory for flexible multibody dynamics. *Journal of Computational and Nonlinear Dynamics 9*(4), 041011.

Benjeddou, A., M. Trindade, and R. Ohayon (1997). A unified beam finite element model for extension and shear piezoelectric actuation mechanisms. *Journal of Intelligent Material Systems and Structures 8*(12), 1012–1025.

Berdichevskii, V. (1979). Variational-asymptotic method of constructing a theory of shells: Pmm vol. 43, no. 4, 1979, pp. 664–687. *Journal of Applied Mathematics and Mechanics 43*(4), 711–736.

Borri, M. and T. Merlini (1986). A large displacement formulation for anisotropic beam analysis. *Meccanica 21*(1), 30–37.

Brillante, C., M. Morandini, and P. Mantegazza (2015). Characterization of beam stiffness matrix with embedded piezoelectric devices via generalized eigenvectors. *International Journal of Solids and Structures 59*, 37–45.

Carrera, E., E. Zappino, and G. Li (2018). Analysis of beams with piezo-patches by node-dependent kinematic finite element method models. *Journal of Intelligent Material Systems and Structures 29*(7), 1379–1393.

Cesnik, C. and R. Palacios (2003). Modeling piezocomposite actuators embedded in slender structures. In *44th AIAA/ASME/ASCE/AHS/ASC Structures, Structural Dynamics, and Materials Conference*, pp. 1803.

Cesnik, C. E. and D. H. Hodges (1997). Vabs: a new concept for composite rotor blade cross-sectional modeling. *Journal of the American helicopter society 42*(1), 27–38.

Chen, P. C. and I. Chopra (1996, feb). Induced strain actuation of composite beams and rotor blades with embedded piezoceramic elements. *Smart Materials and Structures 5*(1), 35–48.

Chopra, I. (2002). Review of state of art of smart structures and integrated systems. *AIAA journal 40*(11), 2145–2187.

Crawley, E. F. and E. H. Anderson (1990). Detailed models of piezoceramic actuation of beams. *Journal of Intelligent Material Systems and Structures 1*(1), 4–25.

Elshafei, M. A. and F. Alraiess (2013). Modeling and analysis of smart piezoelectric beams using simple higher order shear deformation theory. *Smart Materials and Structures 22*(3), 035006.

Eslami, M. R., R. B. Hetnarski, J. Ignaczak, N. Noda, N. Sumi, and Y. Tanigawa (2013). *Theory of elasticity and thermal stresses*, Volume 197. Springer.

Ghiringhelli, G. (1997). On the thermal problem for composite beams using a finite element semi-discretisation. *Composites Part B: Engineering 28*(5-6), 483–495.

Ghiringhelli, G. L., P. Masarati, and P. Mantegazza (1997). Characterisation of anisotropic, non-homogeneous beam sections with embedded piezo-electric materials. *Journal of Intelligent Material Systems and Structures 8*(10), 842–858.

Giavotto, V., M. Borri, P. Mantegazza, G. Ghiringhelli, V. Carmaschi, G. Maffioli, and F. Mussi (1983). Anisotropic beam theory and applications. *Computers & Structures 16*(1-4), 403–413.

Gu, Q., X.-s. Xu, and Y. Leung, Andrew (2005). Application of hamiltonian system for two-dimensional transversely isotropic piezoelectric media. *Journal of Zhejiang University-SCIENCE A 6*(9), 915–921.

Han, S. and O. A. Bauchau (2015). Nonlinear three-dimensional beam theory for flexible multibody dynamics. *Multibody System Dynamics 34*(3), 211–242.

Han, S. and O. A. Bauchau (2016). On saint-venant's problem for helicoidal beams. *Journal of Applied Mechanics 83*(2), 021009.

Hodges, D. H. (2006). *Nonlinear composite beam theory.* American Institute of Aeronautics and Astronautics.

Kapuria, S. and N. Alam (2006). Efficient layerwise finite element model for dynamic analysis of laminated piezoelectric beams. *Computer Methods in Applied Mechanics and Engineering 195*(19-22), 2742–2760.

Kapuria, S., P. Kumari, and J. Nath (2010). Efficient modeling of smart piezoelectric composite laminates: a review. *Acta Mechanica 214*(1-2), 31–48.

Ke, L.-L., Y.-S. Wang, J. Yang, and S. Kitipornchai (2014). The size-dependent vibration of embedded magneto-electro-elastic cylindrical nanoshells. *Smart Materials and Structures 23*(12), 125036.

Kondaiah, P., K. Shankar, and N. Ganesan (2012). Studies on magneto-electro-elastic cantilever beam under thermal environment. *Coupled systems mechanics 1*(2), 205–217.

Kpeky, F., F. Abed-Meraim, H. Boudaoud, and E. M. Daya (2018). Linear and quadratic solid–shell finite elements shb8pse and shb20e for the modeling of piezoelectric sandwich structures. *Mechanics of Advanced Materials and Structures 25*(7), 559–578.

Kreith, F., R. M. Manglik, and M. S. Bohn (2012). *Principles of heat transfer.* Cengage learning.

Loewy, R. G. (1997). Recent developments in smart structures with aeronautical applications. *Smart Materials and Structures 6*(5), R11.

Logg, A., G. N. Wells, and J. Hake (2012). *DOLFIN: a C++/Python Finite Element Library,* Chapter 10. Springer.

Mielke, A. (1988). Saint-venant's problem and semi-inverse solutions in nonlinear elasticity. *Archive for Rational Mechanics and Analysis 102*(3), 205–229.

Mielke, A. (1991). Hamiltonian and lagrangian flows on center manifolds: with applications to elliptic variational problems. *LectureNote in Matematics 1489.*

Morandini, M., M. Chierichetti, and P. Mantegazza (2010). Characteristic behavior of prismatic anisotropic beam via generalized eigenvectors. *International Journal of Solids and Structures 47*(10), 1327–1337.

Noda, N., R. B. Hetnarski, and T. Yoshinobu (2003). *Thermal Stresses* (Second ed.). New York, USA: Taylor & Francis.

Palacios, R. and C. E. S. Cesnik (2005). Cross-sectional analysis of nonhomogeneous anisotropic active slender structures. *AIAA journal 43*(12), 2624–2638.

Rafiee, M., F. Nitzsche, and M. Labrosse (2017). Dynamics, vibration and control of rotating composite beams and blades: A critical review. *Thin-Walled Structures 119,* 795–819.

Reddy, J. N. (1984). A simple higher-order theory for laminated composite plates. *Journal of applied mechanics 51*(4), 745–752.

Roy, S. and W. Yu (2009). A coupled timoshenko model for smart slender structures. *International Journal of Solids and Structures 46*(13), 2547–2555.

Roy, S., W. Yu, and D. Han (2007). An asymptotically correct classical model for smart beams. *International Journal of Solids and Structures 44*(25-26), 8424–8439.

Wang, Q. and W. Yu (2011). Multiphysics modeling of composite beams under large temperature changes. In *53rd AIAA/ASME/ASCE/AHS/ASC Structures, Structural Dynamics and Materials Conference 20th AIAA/ASME/AHS Adaptive Structures Conference 14th AIAA,* pp. 1578.

Wang, Q. and W. Yu (2012). Asymptotic multiphysics modeling of composite slender structures. *Smart Materials and Structures 21*(3), 035002.

Yang, J. (2007). Piezoelectric transformer structural modeling-a review. *IEEE transactions on ultrasonics, ferroelectrics, and frequency control 54*(6), 1154–1170.

Yu, W. (2002). *Variational asymptotic modeling of composite dimensionally reducible structures.* Ph. D. thesis, Georgia Institute of Technology.

Zhong, W., X. Xu, and H. Zhang (1996). Hamiltonian system and the saint venant problem in elasticity. *Applied Mathematics and Mechanics 17*(9), 827–836.